

Enhanced Angular Momentum Transport in Accretion Disks

Steven A. Balbus

Department of Astronomy, VITA, University of Virginia, Charlottesville, VA 22901
sb@virginia.edu

KEYWORDS: accretion, accretion disks, instabilities, MHD, turbulence

ABSTRACT: The status of our current understanding of angular momentum transport in accretion disks is reviewed. The last decade has seen a dramatic increase both in the recognition of key physical processes and in our ability to carry through direct numerical simulations of turbulent flow. Magnetic fields have at once powerful and subtle influences on the behavior of (sufficiently) ionized gas, rendering them directly unstable to free energy gradients. Outwardly decreasing angular velocity profiles are unstable. The breakdown of Keplerian rotation into MHD turbulence may be studied in some numerical detail, and key transport coefficients may be evaluated. Chandra observations of the Galactic Center support the existence of low luminosity accretion, which may ultimately prove amenable to global three-dimensional numerical simulation.

CONTENTS

Introduction	2
Preliminaries	5
<i>Fundamental Equations</i>	5
<i>Nonlinear Fluctuations</i>	6
Hydrodynamic Waves in Disks	7
<i>The Linear Wave Equation</i>	7
<i>Two Dimensional WKB Waves</i>	9
<i>Angular Momentum and Energy Wave Fluxes</i>	12
<i>Wave Angular Momentum Transport in Protoplanetary Disks.</i>	14
<i>Angular Momentum Transport and Weak Turbulence</i>	16
<i>Bending Waves</i>	17
Hydrodynamical Instability	17
MHD Turbulence	21
<i>Introduction</i>	21
<i>The Magnetorotational Instability: A Simple Overview</i>	21
<i>The Magnetorotational Instability: A Brief History</i>	23
<i>General Axisymmetric Stability Criteria</i>	24
<i>Low-Ionization Disks</i>	25
<i>Turbulent Transport in Thin Disks</i>	26
<i>Transport in Low Radiation Accretion Flows</i>	30

arXiv:astro-ph/0306208v1 10 Jun 2003

Numerical Simulations of MHD Disk Turbulence	31
<i>The Local Approximation</i>	31
<i>Radiative Effects</i>	33
<i>Low Ionization Disk Simulations</i>	34
Global Disk Simulations	34
<i>Two-Dimensional Simulations</i>	35
<i>Cylindrical Disks</i>	35
<i>Three-Dimensional Simulations</i>	36
Summary	37

*I hate being “allowed for,” as if
I were some incalculable quantity
in an astronomical equation.*

– *D.L. Sayers*, The Documents in the Case.

1 Introduction

In recent years, accretion disk transport theory has developed so rapidly, any review is destined to be significantly dated the moment it appears in print. This will put the reader at a disadvantage. However, it is an exhilarating time for disk theorists.

The current happy state of affairs in this computationally-driven field is largely due to the swift evolution of three-dimensional magnetohydrodynamical (MHD) codes and their supporting hardware. These powerful tools arrive with provident timing, coinciding with a deepening theoretical understanding of the role of magnetic fields in accretion disk dynamics. The result is that accretion disk turbulence theory has grown from a mere viscosity coefficient to a fully quantitative science. In this review, I will focus on what is now known of the relationship between turbulence and enhanced angular momentum in accretion disks, and the resulting implications for some selected astrophysical systems.

The classical problem with accretion disks is that they do of course accrete. How is it that fluid elements orbiting in a central force field lose their specific angular momentum and spiral inwards? One may quickly rule out ordinary particulate viscosity. Astrophysical disks are simply too big. To fix ideas, note that disturbances are propagated by viscous diffusion over a distance l on a time scale of order l^2/ν , where ν is the kinematic viscosity, or about 3×10^7 years for $l \sim 10^{10}$ cm and $\nu = 10^5$ cm² s⁻¹. This is orders of magnitude too long for the time variability seen in compact object accretion disks.

The way around this difficulty was perceived to be turning the woefully inadequate viscosity to one’s advantage by appealing to the associated large Reynolds number. This, it was thought, would turn differential rotation into shear-driven turbulence (e.g., Crawford & Kraft 1956, Shakura & Sunyaev 1973). The breakdown of shear flow lamina into turbulence was known since the work of Reynolds

to be triggered by nonlinear flow instabilities. The fact that there were no demonstrable local *linear* instabilities for a Keplerian rotation profile was therefore not immediately viewed as an embarrassment to this scenario.

Shear turbulence is a desirable trait in a flows where greatly enhanced (angular) momentum transport is needed. This is because shear-driven turbulence is characterized by a high degree of correlation between the radial and azimuthal velocity fluctuations. This, as we shall see, has the direct effect of raising a disk's angular momentum flux orders of magnitude above what would be possible with an ordinary collisional viscosity.

No topic in fluid dynamics is more contentious than the onset and development of turbulence, and accretion disk turbulence has not been an exception. Keplerian disks do not resemble laboratory shear flows, however locally one peers. Coriolis forces dramatically stabilize rotational flow on large scales and small, a feature not shared by classical *planar* Couette flow or Poiseuille flow.¹ Yet Coriolis forces do no work on the fluid; they are in fact absent from the energy conservation equations. Because a potent free energy source in the form of shear retains a presence with or without Coriolis forces, debate has centered upon whether fluid nonlinearities at a high enough Reynolds number would still find a way to tap into this source when linear disturbances fail to do so.

No published laboratory experiment has shown the breakdown of a Keplerian-like Couette flow profile. But truly definitive studies have yet to be performed. The onset of nonlinear instabilities that have been reported in Couette flow experiments are generally related to very sharp rotational velocity gradients typical of Kelvin-Helmholtz instabilities, not the $r^{-1/2}$ power law characteristic of a Keplerian profile (Triton 1988). The issue is receiving renewed attention, with groups in Saclay, Los Alamos, and Princeton looking at Reynolds numbers $Re \sim 10^{5-6}$, much in excess of those available in the classical experiments (e.g., Coles 1965).

Theoretical developments have been more brisk. A theory for the onset of turbulence in Poiseuille flow was elucidated in the 1970's and 80's (Bayly, Orszag, & Herbert 1988). The key is the existence of neutrally stable (or slowly decaying) finite amplitude disturbances. These solutions are time-steady but spatially periodic in the streamwise direction (Zahn et al. 1974). It is these amended flow profiles that find themselves subject to a rapid, short-wavelength *three-dimensional* instability, leading to a breakdown into turbulence (Orszag & Patera 1980, 1981). A similar process appears to be at work in shear layers (Pierrehumbert & Widnall 1982; Corcos & Lin 1984). It is now generally accepted that the triggering of a rapid, linear three-dimensional instability of a nearly neutrally stable, two-dimensional, finite-amplitude disturbance is a very generic mode of the breakdown of laminar flow into turbulence.

How does this bear on our understanding of accretion disks? The most important point is that even incompressible axisymmetric disturbances in a rotating fluid will propagate in the form of linear inertial waves (Lighthill 1978) with a characteristic frequency proportional to the local vorticity of the rotation profile. Thus, in astrophysical disks, the finite amplitude, neutrally stable axisymmetric state that is critical to the transition to turbulence in mixing layers cannot form.

¹Another key feature that disks do *not* share with these laboratory flows is the presence of a boundary layer at a retaining wall.

Only in a low-vorticity rotational profile, in which the oscillation frequency is much smaller than the shearing rate, would we expect a breakdown of flow lamina into turbulence, similar to what is seen in a mixing layer. This is in good accord with three-dimensional numerical simulations (Balbus, Hawley, & Stone 1996; Hawley, Balbus, & Winters 1999), which find no nonlinear local instabilities in Keplerian disks, but do indeed find that shear layers and low-vorticity disks show a nonlinear breakdown to turbulent flow. There is as yet no analytic proof of local nonaxisymmetric stability, however, and the notion that there may be another nonlinear hydrodynamical route to turbulence in Keplerian disks, beyond the highest resolution available in supercomputer simulations, retains some advocates (Richard & Zahn 1999).

Accretion disks have one critically important attribute not shared with the classical hydrodynamical fluids: they are generally magnetized. By engendering new degrees of freedom in their host fluid, even very weak magnetic fields completely alter the stability behavior of astrophysical gases, both rotationally and thermally (Balbus 2001). Free energy sources in the form of angular velocity and temperature gradients become directly available to destabilize the flow.

The counter-intuitive point here is that a weak magnetic field can have such a potent influence. The stability behavior of strongly magnetized disks is rich and astrophysically interesting (e.g. Terquem & Papaloizou 1996; Varnière & Tagger 2002), but the emphasis in this review is decidedly on subthermal magnetic fields. Rather than depending directly on the strength of the equilibrium magnetic fields, weak field instabilities depend directly upon hydrodynamic properties of the unperturbed disk. If the angular velocity decreases outward in a weakly magnetized accretion disk, which is generally the case, the rotation profile is linearly unstable (Balbus & Hawley 1991). This instability is known as the *magnetorotational instability*, or MRI for short. As we shall see, the physics of the MRI is very simple. Nevertheless, a full understanding of its mathematical generality and wide applicability was much belated, following phenomenological disk theory (Shakura & Sunyaev 1973) by nearly two decades. Knowledge of the instability itself significantly predated modern accretion disk theory (Velikhov 1959), albeit in a rather formal global guise.

The numerical study of the MRI does not require unattainable grid resolutions, and it can be readily simulated. Both local (Hawley, Gammie, & Balbus 1995; Brandenburg et al. 1995) and global (Armitage 1998, Hawley 2000) investigations unambiguously show a breakdown of laminar Keplerian flow into well-developed turbulence. The MRI is the only instability shown to be capable of producing and sustaining the enhanced stress needed for accretion to proceed on viable timescales in non-self-gravitating disks. At low temperatures and high densities, e.g., in the outer regions of cataclysmic variables (Gammie & Menou 1998), or in protostellar disks on AU scales (Gammie 1996) the level of MRI-induced turbulence can change rapidly, erupting or even turning off completely. All this occurs while the underlying Keplerian profile remains essentially fixed. In short, the instability seems capable of the full range of accretion complexity manifested in nature. For all these reasons, despite the difficulties of coping with MHD turbulence, the MRI is now at the center of numerical accretion disk studies.

Let us, however, postpone our discussion of matters magnetic, and turn our attention first to the study of simple hydrodynamical waves in disks. These

are of great practical interest in their own right, especially in protoplanetary disks. But it is also the case that understanding the transport properties of waves deepens one's understanding of turbulent transport, both hydrodynamic and magnetohydrodynamic, and that is our primary reason for reviewing them here. We shall then follow with a discussion of hydrodynamical instability, with a focus on how global instability can in principle emerge in a differentially rotating disk even when the Rayleigh condition is satisfied. Magnetic instability and magnetic turbulence are the topics of the next section. Magnetic stresses are the most important transport mechanism in non self-gravitating disks, provided the gas is minimally ionized to couple to the field. The final two sections are a presentation of recent numerical studies of MHD turbulence, and a summary follows.

2 Preliminaries

2.1 Fundamental Equations

For ease of future reference, we list here the fundamental equations of magnetohydrodynamics.

$$\frac{\partial \rho}{\partial t} + \nabla \cdot (\rho \mathbf{v}) = 0 \quad (1)$$

$$\begin{aligned} \rho \frac{\partial \mathbf{v}}{\partial t} + (\rho \mathbf{v} \cdot \nabla) \mathbf{v} = & -\nabla \left(P + \frac{B^2}{8\pi} \right) - \rho \nabla \Phi + \left(\frac{\mathbf{B} \cdot \nabla}{4\pi} \right) \mathbf{B} \\ & + \eta_V \left(\nabla^2 \mathbf{v} + \frac{1}{3} \nabla (\nabla \cdot \mathbf{v}) \right) \end{aligned} \quad (2)$$

$$\frac{\partial \mathbf{B}}{\partial t} = \nabla \times (\mathbf{v} \times \mathbf{B} - \eta_B \nabla \times \mathbf{B}) \quad (3)$$

$$\frac{P}{\gamma - 1} \frac{d \ln P \rho^{-\gamma}}{dt} = Q^+ - Q^- \quad (4)$$

Equation (1) is mass conservation, (2) is the dynamical equation of motion, (3) is the induction equation, and (4) is the entropy equation. Our notation is standard: ρ is the mass density, \mathbf{v} the fluid velocity, P the pressure (plus radiation pressure when important), Φ the gravitational potential, \mathbf{B} the magnetic field vector, γ is the adiabatic index, Q^+ (Q^-) represent heat gains (losses), η_V the microscopic kinematic shear viscosity, and η_B the microscopic resistivity. The azimuthal component of the equation of motion deserves separate mention, as it is a direct expression of angular momentum conservation:

$$\frac{\partial(\rho R v_\phi)}{\partial t} + \nabla \cdot \left[\rho R v_\phi \mathbf{v} - \frac{R B_\phi}{4\pi} \mathbf{B} + \left(P + \frac{B^2}{8\pi} \right) \mathbf{e}_\phi \right] = 0 \quad (5)$$

where \mathbf{e}_ϕ is a unit vector in the ϕ direction. The dissipative terms have been dropped because they appear only in the flux term, transporting a negligible amount of angular momentum.

It is also useful to have at hand an equation for total energy conversation. This is somewhat lengthy to derive (Balbus & Hawley 1998), but the result is readily

interpreted:

$$\frac{\partial \mathcal{E}}{\partial t} + \nabla \cdot \mathcal{F}_{\mathcal{E}} = -Q^- \quad (6)$$

where the energy density \mathcal{E} is

$$\mathcal{E} = \frac{1}{2}\rho v^2 + \frac{P}{\gamma - 1} + \rho\Phi + \frac{B^2}{8\pi} \quad (7)$$

and the energy flux is

$$\mathcal{F}_{\mathcal{E}} = \mathbf{v} \left(\frac{1}{2}\rho v^2 + \frac{\gamma P}{\gamma - 1} + \rho\Phi \right) + \frac{\mathbf{B}}{4\pi} \times (\mathbf{v} \times \mathbf{B}). \quad (8)$$

The energy density consists of kinetic, thermal, gravitational, and magnetic components; the flux is similar with the magnetic component present as a Poynting flux. The heating term Q^+ , an entropy source, is assumed to arise from microscopic dissipation, and it does not explicitly appear in the total energy equation — it simply converts one form of energy to another. The radiative Q^- term, on the other hand, represents genuine systemic energy losses, and appears explicitly in the conservation equation.

2.2 Nonlinear Fluctuations

Both waves and turbulence involve the concept of well-defined departures of the flow from a smooth background. Velocity fluctuations are of particular interest, because it is possible to formulate an exact energy conservation law for the fluctuations themselves. This, in turn, explicitly shows the role of differential rotation as a source of free energy for the (correlated) turbulent fluctuations associated with outward transport of angular momentum.

Let us define the velocity fluctuation \mathbf{u} by

$$\mathbf{u} = \mathbf{v} - R\Omega(R) \mathbf{e}_{\phi}. \quad (9)$$

Ω is in principle arbitrary, but of course the motivation for this definition is that $\Omega(R)$ is a reasonably good approximation to an underlying rotation profile for the accretion flow. It is possible to combine the equation of motion (2) with the internal entropy equation (4) to obtain an exact, ϕ averaged energy equation for the u velocity fluctuations alone:

$$\frac{\partial \mathcal{E}_u}{\partial t} + \nabla \cdot \mathcal{F}_{\mathcal{E}_u} = - \left(\rho u_R u_{\phi} - \frac{B_R B_{\phi}}{4\pi} \right) \frac{d\Omega}{dR} - Q^-. \quad (10)$$

Here \mathcal{E}_u is the fluctuation energy density

$$\mathcal{E}_u = \frac{1}{2}\rho(u^2 + \Phi_{eff}) + \frac{P}{\gamma - 1} + \frac{B^2}{8\pi}, \quad (11)$$

Φ_{eff} is an effective potential function

$$\Phi_{eff} = \Phi - \int^R R\Omega^2 dR, \quad (12)$$

and $\mathcal{F}_{\mathcal{E}\mathbf{u}}$ is the energy flux of the fluctuations themselves:

$$\mathcal{F}_{\mathcal{E}\mathbf{u}} = \mathbf{u} \left(\frac{1}{2} \rho u^2 + \frac{\gamma P}{\gamma - 1} + \rho \Phi_{eff} \right) + \frac{\mathbf{B}}{4\pi} \times (\mathbf{u} \times \mathbf{B}). \quad (13)$$

Because equation (10) has been averaged over ϕ , only R and Z components appear in the flux.

The combination

$$T_{R\phi} = \rho u_R u_\phi - \frac{B_R B_\phi}{4\pi} \quad (14)$$

is an important quantity in both turbulent and wave transport theories of accretion disks. It has appeared once before: within the angular momentum conservation equation (5), where it emerges as a component in the flux term. Its constituents may be separately identified as Reynolds ($\rho u_R u_\phi$) and Maxwell ($-B_R B_\phi / 4\pi$) stresses. (Note that both wavelike and turbulent disturbances can create tight radial–azimuthal correlations in the velocity and magnetic fields.) These correlations evidently serve two conceptually quite different functions: they directly transport angular momentum, and as shown in equation (10), they tap into the free energy source of differential rotation. The latter role is particularly crucial for sustaining turbulence. Without external driving, the only energy source for the fluctuations is this coupling of the stress to the differential rotation. In astrophysical accretion disks that make use of this free energy source, $T_{R\phi}$ must have the same sign as $-d\Omega/dR$, i.e., it must be positive.

3 Hydrodynamic Waves in Disks

3.1 The Linear Wave Equation

Consider an unmagnetized disk in which the pressure and density obey a simple polytropic equation of state, $P = K\rho^\gamma$, where K is a constant. We may define an enthalpy function \mathcal{H} :

$$\mathcal{H} = \int \frac{dP}{\rho} = \frac{\gamma P / \rho}{\gamma - 1} = \frac{a^2}{\gamma - 1}, \quad (15)$$

where a^2 is the adiabatic sound speed. It is convenient to work in standard cylindrical coordinates (R, ϕ, Z) . The gas rotates in the gravitational field of a central mass. The angular velocity Ω must be constant on cylinders, $\Omega = \Omega(R)$ (Tassoul 1978).

Although it is a standard approximation, the assumption of a barotropic equation of state is obviously an idealization. Among other shortcomings, it precludes the possibility of a buoyant response in the form of internal gravity waves due to Brunt-Väisälä oscillations (Ogilvie & Lubow 1999). But in standard disk models, entropy stratification arises because of radiative heat diffusion from turbulent heating. A linearized wave treatment of such an “equilibrium” is at best a delicate matter. In general, the vertical temperature structure of accretion disks is not well-understood, and the virtue of adopting a barotropic pressure is that it allows important dynamical behavior to be revealed.

Our goal is to study how linearized wave disturbances transport energy and angular momentum through a Keplerian disk. To this end, we introduce small

perturbations to the equilibrium solution, denoted as $\delta\rho$, $\delta\mathbf{v}$, etc. The equilibrium solution is axisymmetric, so a perturbed flow quantity X has the form

$$\delta X = \delta X(R, Z) \exp(im\phi - i\omega t), \quad (16)$$

where m is an integer and ω is the wave frequency. For the moment, the R, Z dependence of the amplitude is unrestricted. The linearized dynamical equations of motion are

$$-i\bar{\omega} \delta v_R - 2\Omega \delta v_\phi = -\frac{\partial \delta \mathcal{H}}{\partial R} \quad (17)$$

$$-i\bar{\omega} \delta v_\phi + \frac{\kappa^2}{2\Omega} \delta v_R = -i\frac{m}{R} \delta \mathcal{H} \quad (18)$$

$$-i\bar{\omega} \delta v_Z = -\frac{\partial \delta \mathcal{H}}{\partial Z}. \quad (19)$$

We have introduced the Doppler-shifted wave frequency,

$$\bar{\omega} = \omega - m\Omega, \quad (20)$$

and what is known as the epicyclic frequency κ :

$$\kappa^2 = 4\Omega^2 + \frac{d\Omega^2}{d \ln R}. \quad (21)$$

The epicyclic frequency is the rate at which a point mass in a circular motion, disturbed in the plane of its orbit, would oscillate about its average radial location (Binney & Tremaine 1987). A negative value of κ^2 quite generally implies that axisymmetric disturbances are hydrodynamically unstable. The requirement $\kappa^2 > 0$ is known as the Rayleigh stability criterion.

The remaining equations are the linearized mass conservation equation

$$-i\bar{\omega} \frac{\delta \rho}{\rho} + \frac{1}{\rho} \nabla \cdot (\rho \delta \mathbf{v}) = 0. \quad (22)$$

and the equation of state (relating density and enthalpy perturbations):

$$\delta \mathcal{H} = a^2 \frac{\delta \rho}{\rho} \quad (23)$$

The three dynamical equations may be solved for $\delta \mathbf{v}$ in terms of $\delta \mathcal{H}$:

$$\delta v_R = \frac{i}{D} \left[\bar{\omega} \frac{\partial \delta \mathcal{H}}{\partial R} - \frac{2\Omega m}{R} \delta \mathcal{H} \right], \quad (24)$$

$$\delta v_\phi = \frac{1}{D} \left[\frac{\kappa^2}{2\Omega} \frac{\partial \delta \mathcal{H}}{\partial R} - \frac{m\bar{\omega}}{R} \delta \mathcal{H} \right], \quad (25)$$

$$\delta v_Z = -\frac{i}{\bar{\omega}} \frac{\partial \delta \mathcal{H}}{\partial Z}, \quad (26)$$

where

$$D = \kappa^2 - \bar{\omega}^2. \quad (27)$$

Using equations (24 – 26) in (22) and simplifying the results, one obtains the linear wave equation for the disk:

$$\left[\frac{1}{R} \frac{\partial}{\partial R} \left(\frac{R\rho}{D} \frac{\partial}{\partial R} \right) - \frac{1}{\bar{\omega}^2} \frac{\partial}{\partial Z} \left(\rho \frac{\partial}{\partial Z} \right) - \frac{m^2 \rho}{R^2 D} + \frac{1}{R\bar{\omega}} \frac{\partial}{\partial R} \left(\frac{2\Omega m \rho}{D} \right) + \frac{\rho}{\epsilon^2 a^2} \right] \delta\mathcal{H} = 0 \quad (28)$$

We have inserted an artificial ϵ factor in the sound speed term, which, though formally equal to unity, will be used as an aid for sorting out asymptotic orders in a WKB analysis. (The disk is here presumed to be cold in the sense that $R\Omega \gg a$.)

The locations at which $D = 0$ and $\bar{\omega} = 0$ are singularities of the wave equation, though in the case of the former the singularity is only apparent, not real. They are known respectively as Lindblad and corotation resonances, and their neighborhoods are zones where waves couple strongly to the disk. They are of importance in the study of tidally driven waves, and are critical to an understanding of planetary migration (Goldreich & Tremaine 1979, 1980; Ward 1997). In this section, our emphasis will be upon freely propagating WKB waves, and we shall assume that neither D nor $\bar{\omega}$ is small; *i.e.*, that we are not in the neighborhood of resonance.

3.2 Two Dimensional WKB Waves

3.2.1 First Order: Dispersion Relation and Group Velocity

We seek solutions of equation (28) having the form

$$\delta\mathcal{H} = A(R, Z) \exp \left[\frac{iS(R, Z)}{\epsilon} \right] \quad (29)$$

The idea is that the phase S/ϵ varies rapidly, and the ϵ factor ensures this in the formal limit $\epsilon \rightarrow 0$. We will solve the wave equation to leading and second order in a $1/\epsilon$ expansion. Note that the absolute phase is not relevant here, and we may assume that A , the amplitude, is real. We shall also assume that the waves are tightly wound, *i.e.* that both k_R and $k_Z \gg m/R$.

Inserting (29) into (28), we find that the leading order $1/\epsilon^2$ terms give

$$\frac{k_Z^2}{\bar{\omega}^2} + \frac{k_R^2}{\bar{\omega}^2 - \kappa^2} = \frac{1}{a^2}, \quad (30)$$

where

$$(k_R, k_Z) = (\partial S / \partial R, \partial S / \partial Z). \quad (31)$$

This is the dispersion relation for WKB disk waves, and the gradients of S are, in essence, the wavenumber components.

Figure (1) is a plot of the constant frequency curves in the $k_Z a, k_R a$ wavenumber plane. For $\bar{\omega} > \kappa$, the iso- $\bar{\omega}$ curves are ellipses; for $\bar{\omega} < \kappa$, they are hyperbolae. These two different conic sections define the two distinct wave branches, with very different transport properties. Indeed, this diagram makes evident several remarkable features of disk waves.

The elliptical iso- $\bar{\omega}$ surfaces correspond to density waves, which are rotationally modified sound waves (e.g Goldreich & Tremaine 1979), and the hyperbolae correspond to inertial waves (Vishniac & Diamond 1989), described below. It is not difficult to show that the ellipses and hyperbolae always intersect at right angles, so that the curves are like a conformal mapping. The practical relevance of this is that since the wave group velocity \mathbf{U} is the wavenumber gradient of $\bar{\omega}$,

$$\mathbf{U} = \left(\frac{\partial \bar{\omega}}{\partial k_R}, \frac{\partial \bar{\omega}}{\partial k_Z} \right), \quad (32)$$

the group velocity direction of the density waves lies along the inertial wave iso- $\bar{\omega}$ curves, and the group velocity direction of the inertial waves lies along the density wave curves. Low frequency disturbances in disks have very different transport properties from high frequency disturbances, a point to which we shall return many times.

For a given wavevector (k_R, k_Z) , the gradient to an iso- $\bar{\omega}$ curve could point in either direction, because the dispersion relation (30) does not uniquely determine the sign of $\bar{\omega}$. Direct calculation reveals:

$$U_R \equiv \frac{\partial \bar{\omega}}{\partial k_R} = -\frac{k_R/\bar{\omega}D}{(k_R/D)^2 + (k_Z/\bar{\omega}^2)^2}, \quad (33)$$

$$U_Z \equiv \frac{\partial \bar{\omega}}{\partial k_Z} = \frac{k_Z/\bar{\omega}^3}{(k_R/D)^2 + (k_Z/\bar{\omega}^2)^2}, \quad (34)$$

and

$$\mathbf{k} \cdot \mathbf{U} = \left[a^2 \bar{\omega} \left(k_R^2/D^2 + k_Z^2/\bar{\omega}^4 \right) \right]^{-1} \quad (35)$$

The sign of the group velocity must be carefully determined; it depends upon \mathbf{k} , $\bar{\omega}$, and D . By way of illustration, assume that the wavenumber components are all positive. If Ω decreases with increasing R , density waves ($D < 0$) beyond the corotation radius will propagate radially outward, and radially inward inside of corotation. They will propagate upwards outside corotation, and downwards inside corotation. Inertial waves ($D > 0$) propagate in the *opposite* radial sense as density waves, but in the same vertical direction. Finally, the epicyclic response $D = 0$ is degenerate, and k_R must vanish at this location, the Lindblad resonance. The WKB treatment breaks down here, and other techniques must be used (Goldreich & Tremaine 1979).

3.2.2 Density Waves

The general dispersion relation can be written in the form

$$\bar{\omega}^4 - (k^2 a^2 + \kappa^2) \bar{\omega}^2 + \kappa^2 k_Z^2 a^2 = 0 \quad (36)$$

where $k^2 = k_R^2 + k_Z^2$. In this form the density and inertial wave branches separate cleanly, with the density wave corresponding to a dominant balance between the first two terms in (36), and inertial waves between the final two terms. The density wave branch of the dispersion relation (30) is thus,

$$\bar{\omega}^2 = k^2 a^2 + \kappa^2. \quad (37)$$

The condition that the final term in the dispersion relation be small compared with the first two can be met either if $ka \gg \kappa$, in which case the problem reduces to ordinary acoustic waves, or if $k_Z \ll k_R$, which is the classical one-dimensional density wave problem. In either case, the density wave group velocity \mathbf{U} tends to be parallel to \mathbf{k} , and thus perpendicular to constant phase surfaces.

3.2.3 Inertial Waves

Inertial waves may be less familiar than their density wave counterparts because of the latter's well-known role in the theory of galactic spiral structure. Indeed, as we have just seen, inertial waves disappear entirely in a "thin" disk with $k_Z = 0$, which doubtless contributed to their undeserved second-class role. It must be emphasized that inertial waves are the only avenue of response available to a polytropic disk at driving frequencies less than κ , and the properties of these waves are worthy of attention.

The inertial wave branch cleanly separates from the density wave branch in the limit $k_Z a \gg \kappa$, and is essentially incompressible. Inertial waves satisfy the dispersion relation (36) with the dominant balance attained in the last terms, obtained in the $a \rightarrow \infty$ limit:

$$\bar{\omega}^2 = \frac{k_Z^2}{k_R^2 + k_Z^2} \kappa^2. \quad (38)$$

(Note that WKB inertial waves do not require $R\Omega \gg a$.) Equation (38) tells us that only the vertical component of the wave number contributes to the inertial response. This is readily understood: since incompressible fluid displacements are nearly perpendicular to their wavevectors, it is only the planar component of the *displacement* that elicits an inertial response. It is the inertial Coriolis force that provides the return impetus in this class of wave; such forces are accessed only by displacements in the disk plane.

For an inertial wave, $\mathbf{k} \cdot \mathbf{U}$ will typically be of order $\kappa^3/k_Z^2 a^2$, and is thus very small, $\mathbf{k} \cdot \mathbf{U} \ll kU$. Since \mathbf{k} is by definition perpendicular to constant phase surfaces, the inertial wave group velocity lies entirely within these same surfaces. Unlike density waves, which radiate ringlike from their point of origin, inertial waves have the unusual property that they exude, tube-like, slowly establishing their pattern. Driven incompressible turbulence in an otherwise stable hydrodynamic disk is basically an ensemble of interacting inertial waves.

3.2.4 Second Order: Wave Action Conservation

We move to the next order in our WKB analysis. If we gather the terms of order $1/\epsilon$ that arise from substituting (29) into (28), we find that they may be combined into the form of an exact divergence:

$$\frac{\partial}{\partial Z} \left[\frac{\rho k_Z A^2}{\bar{\omega}^2} \right] - \frac{1}{R} \frac{\partial}{\partial R} \left[R \left(\frac{\rho k_R A^2}{D} \right) \right] = 0, \quad (39)$$

or

$$\nabla \cdot \left[\rho A^2 \bar{\omega} \left(k_R^2/D^2 + k_Z^2/\bar{\omega}^4 \right) \mathbf{U} \right] = 0. \quad (40)$$

This expresses the conservation of wave action, and the quantity multiplying the group velocity vector \mathbf{U} is thus (up to an overall sign) the wave action density. In the next section, we will show that the wave action is proportional not to the wave energy, which is not a conserved quantity (unless $m = 0$), but to the wave angular momentum. Except at resonances, this is always conserved in a dissipationless fluid.

3.3 Angular Momentum and Energy Wave Fluxes

The wave angular momentum flux is given by

$$\mathcal{F}_{\mathcal{J}} = \rho R \langle \text{Re}(\delta v_{\phi}) \text{Re}(\delta \mathbf{v}) \rangle \quad (41)$$

where the angle brackets denote an average over one wave cycle, and Re denotes the real part. (Hereafter, in all expressions quadratic in the δ wave amplitudes, it is understood that the real part is to be taken, unless explicitly written otherwise.) Note that if the waves could impart a mean mass flux \dot{m} to the background, such terms would produce a contribution to the angular momentum flux of the form $\dot{m} R v_{\phi}$. However, the dissipationless passage of a density or inertial wave does not cause matter to flow in the disk, despite the fact that

$$\langle \delta \rho \delta v_R \rangle \neq 0.$$

This is because the perturbed quantities have been calculated only to linear order in their amplitudes, whereas the fluxes of interest are *second order* in the same amplitudes. Thus, the perturbed velocity is not really $\delta \mathbf{v}$, but $\delta \mathbf{v} + \mathbf{v}_2$, where \mathbf{v}_2 includes all higher order corrections in the velocity amplitude. These need not be wave-like. It is only when \mathbf{v}_2 is included, making a second order contribution to the mass flux as a product with the equilibrium density ρ_0 , that the mass flux disappears:

$$\langle \delta \rho \delta v_R \rangle + \langle \rho_0 v_{2R} \rangle = 0.$$

Fortunately, \mathbf{v}_2 itself does not have to be computed explicitly. Instead, one simply requires $\langle \rho \mathbf{v} \rangle$ to vanish, while retaining all other leading order terms. These will be quadratic in the linear amplitudes; no other second order perturbations subsequently appear. (This is *not* true of dissipational flow, turbulent or wavelike, where mass accretion is clearly a possibility.) In the end, we shall see that all wave fluxes of interest are directly proportional to a conserved wave action.

To determine more precisely the relationship between the wave action and angular momentum, let us calculate the radial component of the angular momentum flux. Using equations (24) and (25), it is straightforward to show that the radial component of the angle momentum flux is

$$\rho R \langle \delta v_R \delta v_{\phi} \rangle = -\frac{m \rho k_R}{D} \frac{A^2}{2} = \frac{m \rho k_R}{\bar{\omega}^2 - \kappa^2} \frac{A^2}{2}. \quad (42)$$

The factor of 1/2 comes from averaging over a wave cycle. Reference to equation (39) shows that this is exactly the radial component of the wave action, multiplied by the proportionality constant $m/2$. It is often useful to express this flux in terms of radial velocity fluctuations. This can be done with the help of equation (24),

neglecting the m term in the WKB limit:

$$\rho R \langle \delta v_R \delta v_\phi \rangle = \rho \frac{m}{k_R} \left(1 - \frac{\kappa^2}{\bar{\omega}^2} \right) \langle (\delta v_R)^2 \rangle. \quad (43)$$

The Z component of the angular momentum flux need not be directly computed, but instead can be obtained by multiplying the radial flux component by the wave group velocity ratio U_Z/U_R :

$$\rho R \langle \delta v_Z \delta v_\phi \rangle = \frac{m \rho k_Z A^2}{\bar{\omega}^2} \frac{1}{2} = \frac{m \rho}{k_Z} \langle (\delta v_Z)^2 \rangle, \quad (44)$$

and therefore

$$\rho R \langle \delta \mathbf{v} \delta v_\phi \rangle = \frac{m \rho A^2}{2} \left(-\frac{k_R}{D}, \frac{k_Z}{\bar{\omega}^2} \right). \quad (45)$$

Equation (45), together with wave action conservation (39), ensure that angular momentum flux is conserved,

$$\nabla \cdot [\rho R \langle \delta \mathbf{v} \delta v_\phi \rangle] = 0, \quad (46)$$

as embodied in (5).

How does this bear on energy conservation? Although the total mechanical energy of the disk-wave system must be conserved (absent dissipation), wave energy is *not*, in general, conserved. The rate at which wave energy is exchanged with the disk's differential rotation is in fact

$$\text{volumetric energy exchange rate} = -\rho \langle \delta v_R \delta v_\phi \rangle \frac{d\Omega}{d \ln R}, \quad (47)$$

i.e., the exchange rate is “stress by strain,” as per equation (10). An explicit calculation of this is revealing, however.

Equation (8) and the requirement of vanishing mass flow leave

$$\mathcal{F}_\mathcal{E} = \left(\frac{1}{2} \rho v^2 + \frac{\gamma P}{\gamma - 1} \right) \mathbf{v} \quad (48)$$

as the contributing energy flux terms. The first term is the contribution from the background, and it vanishes in a comoving frame. The second, representing the wave itself, is the enthalpy flux. Once again, since no contribution to the enthalpy flux can come directly from mass flow, only one term quadratic in the wave amplitudes survives the averaging procedure:

$$\langle P \mathbf{v} \rangle = \left\langle \rho \left(\frac{P}{\rho} \right) \mathbf{v} \right\rangle \rightarrow \rho \left\langle \delta \left(\frac{P}{\rho} \right) \delta \mathbf{v} \right\rangle. \quad (49)$$

Now, for a polytropic equation of state,

$$\delta \left(\frac{P}{\rho} \right) = \frac{\gamma - 1}{\gamma} \frac{\delta P}{\rho}, \quad (50)$$

hence the wave (enthalpy) flux is just

$$\mathcal{F}_\mathcal{E} (\text{wave}) = \langle \delta P \delta \mathbf{v} \rangle = \rho \langle \delta \mathcal{H} \delta \mathbf{v} \rangle. \quad (51)$$

This is a general and well-known result that can be derived in other ways (e.g. Lighthill 1978). From equations (24)–(26), we use the leading order WKB terms, which combine to give the (R, Z) components of the flux:

$$\rho\langle\delta\mathcal{H}\delta\mathbf{v}\rangle = \frac{\bar{\omega}\rho A^2}{2} \left(-\frac{k_R}{D}, \frac{k_Z}{\bar{\omega}^2}\right) = \frac{\bar{\omega}}{m}\rho R\langle\delta v_\phi\delta\mathbf{v}\rangle \quad (52)$$

This is the mechanical analogue of the wave quantum condition: the wave energy is the product of the wave frequency and the quantized angular momentum unit. Note that the relevant frequency is Doppler shifted relative to the moving medium, as a comoving observer in the disk would measure it. Wave action conservation (46) now gives directly

$$\nabla\cdot[\rho\langle\delta\mathcal{H}\delta\mathbf{v}\rangle] = \frac{d(\bar{\omega}/m)}{dR}\rho R\langle\delta v_\phi\delta v_R\rangle = -\rho\langle\delta v_\phi\delta v_R\rangle\frac{d\Omega}{d\ln R}, \quad (53)$$

which shows that the wave energy grows at a rate given by the stress-by-strain formula (47).

To verify that the total energy of the disk and wave system is conserved, we return to the energy flux (48). Using “no mass flux” reasoning similar to that used for determining the enthalpy wave flux, the kinetic energy flux becomes

$$\frac{1}{2}\rho v^2\mathbf{v} \rightarrow \rho R\Omega\langle\delta v_\phi\delta\mathbf{v}\rangle, \quad (54)$$

so that it, too, is just proportional to the angular momentum flux. The net energy flux of the wave plus the background kinetic energy flux is

$$\rho R\langle\delta v_\phi\delta\mathbf{v}\rangle \left(\frac{\bar{\omega}}{m} + \Omega\right) = \frac{\omega}{m}\rho R\langle\delta v_\phi\delta\mathbf{v}\rangle \quad (55)$$

Since ω is constant, wave action (or angular momentum) conservation guarantees that this quantity, the total energy flux, is likewise conserved.

The following summary statements can be made: (1) Wave action and wave angular momentum flux are both conserved quantities. (2) The wave energy flux is related to wave angular momentum flux by

$$\mathcal{F}_\mathcal{E} \text{ (wave)} = \frac{\bar{\omega}}{m}\mathcal{F}_\mathcal{J} = \frac{\bar{\omega}}{m}\rho R\langle\delta v_\phi\delta\mathbf{v}\rangle, \quad (56)$$

and is *not* conserved. (3) The total energy flux of the wave plus background is related to the wave angular momentum flux by

$$\mathcal{F}_\mathcal{E} \text{ (total)} = \frac{\omega}{m}\mathcal{F}_\mathcal{J} = \frac{\omega}{m}\rho R\langle\delta v_\phi\delta\mathbf{v}\rangle, \quad (57)$$

and *is* conserved. Wave action, angular momentum flux, and total energy flux are all essentially the same thing, differing from one another only by constant proportionality factors.

3.4 Wave Angular Momentum Transport in Protoplanetary Disks.

In any shearing disk, local nonaxisymmetric disturbances tend to evolve toward a trailing configuration: a wave crest advances in R as it decreases, or trails, in

ϕ . This is an obvious consequence of an outwardly decreasing rotation profile; leading configurations are created when the angular velocity increases outward. Since $m d\phi + k_R dR = 0$ along a constant phase path, m and k_R must have the same sign in a trailing wave form. From this result and equation (43), it follows that *trailing density waves transport angular momentum radially outward, while trailing inertial waves transport angular momentum radially inward*. This is a conclusion of some astrophysical significance.

One of the most interesting and important applications of wave angular momentum transport occurs in protoplanetary disks. A planet embedded in such a disk will tidally excite density waves in regions where $\bar{\omega}^2 > \kappa^2$. (Goldreich & Tremaine 1979, 1980). Though the wave group velocity and energy flux will differ in sign on either side of the planet's orbit, the angular momentum flux will always be directed outwards. There are then two questions that immediately arise: (1) Will the planet lose enough angular momentum to the waves that it will eventually be accreted by the central star? (2) Is this an effective angular momentum transport mechanism for the disk?

Whether the planet loses or gains angular momentum depends upon the symmetry of the angular momentum transfer. The locations at which D vanishes, the Lindblad resonances, are the launching points of the density waves. The fundamental frequency of the driving potential is of course just the planetary orbit frequency Ω_p , but there are Fourier components at all integer multiples $\omega = m\Omega_p$. Hence the Lindblad resonances are defined by

$$\Omega_p - \Omega = \pm\kappa/m$$

or

$$r = \left(\frac{m \pm 1}{m}\right)^{2/3} r_p, \quad (58)$$

where r_p is the planet's location. The outer resonances thus tend to be somewhat closer to the planet than the inner resonances (Goldreich & Tremaine 1980, Ward 1986) with the consequence that angular momentum is lost to the disk, and the planet migrates inwards. The time scale for orbital evolution is embarrassingly rapid: if the present day Jupiter were at its current location in a disk at a temperature of 100 K and a column density of 100 g cm^{-2} , its orbit would evolve in a few thousand years!

Once the interaction between the planet and the mass becomes nonlinear, material within the planet's Roche lobe is efficiently evacuated, and a gap forms (Lin & Papaloizou 1979). Material inside the planet loses angular momentum and falls in, whereas material outside the planet acquires angular momentum and moves out. The subsequent evolution of the planet then follows that of the disk itself, and the planet moves in on the timescale of the accretion process. In standard disk models (Hartmann et al. 1998), this also is rapid compared with the disk's lifetime.

It is not an easy matter to go beyond these simple estimates, and the problem of how to halt migration is a serious one. Torques exerted at the location of the planet itself (corotation) could conceivably help, but these are difficult to evaluate, as are the complications associated with magnetic couplings, should these be present (Nelson & Papaloizou 2003). It is also possible that a gap may

open in a quiescent disk region near the midplane, while accretion occurs via a magnetically active envelope (Gammie 1996).

The question of whether an ensemble of planets embedded in a disk might serve as an effective viscosity has been examined recently by Goodman & Rafikov (2001). The idea is that density waves would dissipate locally, but also transport energy and angular momentum like a kinematic viscosity. Goodman & Rafikov argue that if all the dust in the solar nebula were gathered into an ensemble of Earth-like planets, the effective Reynolds number (using the sound speed and a vertical scale height) of the planet-gas fluid would be 10^3 – 10^4 . As noted by these authors, however, even Earth-mass planets migrate rapidly, and are also thought to form only late in the disk’s evolution. The nature of angular momentum transport in protostellar/planetary disks remains very much open.

3.5 *Angular Momentum Transport and Weak Turbulence*

For a given mass and angular momentum, the lowest energy configuration of a disk is not a disk at all, but a singular state in which all the mass is at the center and all the angular momentum is at infinity (borne by a negligible amount of mass). The ubiquitous appearance of trailing density waves in spiral galaxies is understood as an attempt to reach this minimum energy state (Lynden-Bell & Kalnajs 1972).

Now self-gravitating density waves, unlike those considered here, are not restricted to values of $\bar{\omega} > \kappa$. But without self-gravity, *any* trailing wave disturbance with a comoving frequency less than the local epicyclic frequency will drive angular momentum “the wrong way,” inward, and will not move the disk toward its ultimate minimum energy state. This statement depends only upon the wave’s trailing nature; the group velocity, for example, could have either sign. Only trailing, compressive disturbances transport angular momentum outward, and absent a powerful organizer like self-gravity, these are expensive to excite and maintain.

Whether one envisions hydrodynamical disk turbulence as an ensemble of interacting waves, or more phenomenologically as dissipative mixing of fluid elements, the tendency is for angular momentum to go inwards. To understand the case for the latter, consider the mixing of two different fluid elements, *A* and *B*, with *A* originating farther out in the disk. When they meet at some intermediate radius, *A* will tend to have higher angular momentum than *B*, since angular momentum increases outward in a Rayleigh-stable disk. When it is at the same radius as *B*, *A* will necessarily have a higher angular velocity, and angular momentum will be transported from *A* to *B* if the mixing lowers the energy (Balbus 2000). In other words, dissipative mixing transports angular momentum inwards. (Note that rigorous specific angular momentum conservation by the displaced fluid elements is not essential to this argument.)

This wave behavior may be the explanation behind the finding of numerical simulations showing that local inward angular momentum transport generally ensues when turbulence in Keplerian disks is driven externally (Stone & Balbus 1996, Cabot 1996), but that vigorous disturbances can in fact drive outward angular momentum transport. We have just argued that direct turbulent transport

from fluid element mixing is itself likely to result in inward transport. It is also likely, however, that unstable convective modes will mix with and excite stable wave modes, since only a rather small subset of wavenumbers are formally unstable. Incompressible convection couples more strongly to inertial waves than to density waves. The resulting sheared, trailing wave forms would transport angular momentum inwards. By way of contrast, vigorously driven convection on sufficiently rapid timescales (faster than the sound crossing time over a vertical scale-height), can couple directly to compressive *density waves*, whose trailing configurations transport angular momentum outwards. Note that thermal convection does not itself carry an “inward transport” label, a point that has been misunderstood. Any agitation in an incompressible Keplerian disk will likely result in inward turbulent transport. Moreover, if trailing wave disturbances bear the brunt of the angular momentum transport in a nonmagnetized disk, the sign of the radial flux depends only upon the ratio of the epicyclic frequency to the wave frequency. Long period, incompressible disturbances transport angular momentum inwards; rapid, compressible disturbances transport outwards.

3.6 Bending Waves

Radial excursions from a circular orbit cause fluid elements to oscillate about their equilibrium point at the epicyclic frequency. A similar frequency κ_Z exists for vertical excursions,

$$\kappa_Z^2 = \frac{\partial^2 \Phi}{\partial Z^2} \quad (59)$$

where Φ is the gravitational potential at the unperturbed (midplane) position of the fluid element (Binney & Tremaine 1987). In conjunction with pressure and rotational forces, these can appear as waves at radial wavelengths much in excess of the disk thickness, and are a possible source of angular momentum transport in an otherwise inviscid disk (Papaloizou & Terquem 1995). The large m/Rk_R ratio of these “bending waves” suggests that they may transport efficiently. Moreover, $m = 1$ modes in non self-gravitating Keplerian-like disks have been shown by Papaloizou & Lin (1994) to propagate with a non-dispersive group velocity.

Papaloizou & Terquem (1995) calculated the angular momentum transport associated with these waves in binary systems in which the companion does not orbit in the disk plane. Like density waves, bending waves grow in amplitude as they approach the center of a disk. This is just conservation of wave action, but it is more intuitively grasped if one thinks of angular momentum conservation and a shrinking radius. If the amplitude becomes nonlinear, it will tend to dissipate, so that the effect is a sort of nonlocal disk viscosity. Typical accretion times in binary systems were found to be at least a few times 10^7 years, at the upper end of estimated disk lifetimes (Hartman 1998). If noncoplaner tidal interactions are common, warps in protostellar disks may influence their evolution.

4 Hydrodynamical Instability

In the Introduction, we discussed the history of invoking high Reynolds number shear turbulence as a source for enhanced accretion disk viscosity. These invocations ignore the stabilizing influence of a positive angular momentum gradient. It

is occasionally argued that this is just a matter of scale, that stabilizing Coriolis forces are less effective at very small scales, and that the appearance of nonlinear instability requires higher Reynolds numbers to observe than are obtainable with current numerical codes (Longaretti 2002). But there are no defining scales when the shear is treated as homogeneous and the Coriolis parameter is treated as a local constant. The stabilization is completely scale-free, which is why both inertial wave propagation, and the Rayleigh stability criterion are independent of wavenumber magnitude (cf. eq. [38]). Any local behavior evinced on small scales in an inviscid shear flow should be seen at larger scales, whether or not Coriolis forces are present.

The most detailed study of three-dimensional local Keplerian stability is that of Hawley, Balbus, & Winters (1999). Both ZEUS and PPM codes (which have very different dispersion properties) were run on the same initial sets of finite-amplitude disturbances, and complete convergence was achieved. Resolutions up to 256^3 grid points were followed. No evidence of nonlinear instability was found.

By way of contrast, shear layers and local constant angular momentum disks, which should exhibit nonlinear instability on all scales, were reported by Hawley et al. (1999) to do just that, even at crude resolutions. This study is compelling evidence that Keplerian disks are not prone to local nonlinear shear instabilities. The results of the last section show that all localized internal disturbances in such disks propagate as WKB waves. Global perturbations that include boundary dynamics can behave quite differently, however, leading not to wave propagation, but to true instability—even if there is no violation of the Rayleigh stability criterion.

Here we will look at the simplest manifestation of global instability, normally a rather complicated process. This class of instability, first studied by Papaloizou & Pringle (1984, 1985), and later elucidated by Goldreich, Goodman, & Narayan (1986), emerges when trapped waves on either side of a corotation region are able to communicate with one another. Typically, on either side of the divide, nonaxisymmetric waves will carry opposite signs in their energy densities: one raises the local disk energy density, the other lowers it. If energy is lost from the negative energy wave and picked up by its positive energy counterpart, *both* amplitudes grow, and as the energy transfer rate increases, the makings of an instability are at hand.

One way to incorporate global physics into a disk problem is to make the boundaries practically local. We therefore consider a radially thin disk with no vertical structure, rather like a thin pipe or drinking straw. The central radius is R_0 , the radial variable is $x = R - R_0$. We may approximate a power law angular velocity profile $\Omega \sim R^{-q}$ as locally linear. With $\Omega_0 = \Omega(R_0)$, the angular velocity is

$$\Omega = \Omega_0(1 - qx/R_0) \quad (60)$$

over the radial extent of our structure, $R = R_0 \pm s$. We retain only the leading order terms in s/R .

The equilibrium solution satisfies

$$-R\Omega^2(R) = -\frac{1}{\rho} \frac{dP}{dR} - \frac{GM}{R^2} \quad (61)$$

To leading order, the equilibrium equation becomes

$$\frac{1}{\rho} \frac{dP}{dR} = \frac{d\mathcal{H}}{dx} = -(2q - 3)\Omega^2 x \quad (62)$$

where \mathcal{H} is the enthalpy function.

Consider Eulerian perturbations to the equilibrium, which are denoted by δ . We use the locally Cartesian azimuthal variable $dy = R d\phi$, and seek plane wave solutions of the form

$$\delta \mathbf{u}(x, y, t) = \delta \mathbf{u}(x) \exp[ik(y - R\Omega_0 t) - i\omega t] \quad (63)$$

where k is the azimuthal wavenumber. We shall consider incompressible disturbances only. The linearized equations of motion are then mass conservation,

$$\frac{d(\delta u_x)}{dx} + ik \delta u_y = 0 \quad (64)$$

and the equations of motion,

$$-i(\omega + q\Omega kx) \delta u_x - 2\Omega \delta u_y = -\frac{d(\delta \mathcal{H})}{dx} \quad (65)$$

$$-i(\omega + q\Omega kx) \delta u_y + \frac{\kappa^2}{2\Omega} \delta u_x = -ik \delta \mathcal{H} \quad (66)$$

These may be combined to give a simple equation for δu_x :

$$\frac{d^2(\delta u_x)}{dx^2} - k^2 \delta u_x = 0. \quad (67)$$

The eigensolutions are thus of the form

$$\delta u_x = C \cosh(kx) + S \sinh(kx). \quad (68)$$

The boundary condition for our problem is that the Langrangian pressure perturbation must vanish at each free surface. Since ρ is constant, this becomes

$$\Delta \mathcal{H} = \delta \mathcal{H} + \xi \frac{d\mathcal{H}}{dx} = 0 \quad (69)$$

where ξ is the radial displacement at the boundary,

$$\xi = \frac{\delta u_x}{-i(\omega + q\Omega kx)}, \quad (70)$$

and $\delta \mathcal{H}$ is given by the azimuthal equation of motion (66). The boundary condition may then be written

$$(\omega + q\Omega kx)^2 \frac{d(\delta u_x)}{dx} + \left[k(\omega + q\Omega kx) \frac{\kappa^2}{2\Omega} + k^2 \mathcal{H}' \right] \delta u_x = 0, \quad (71)$$

where \mathcal{H}' is the equilibrium enthalpy gradient, (62). This constraint, which must be applied at $x = \pm s$, embodies the real dynamical content of the problem. Carrying through this exercise to leading order in ks and solving for ω leads to the dispersion relation

$$\omega^4 - \Omega^2 \omega^2 + 3(3 - q^2)k^2 s^2 \Omega^4 = 0. \quad (72)$$

In the small k limit, the unstable root of (72) is

$$\omega = iks\sqrt{3(q^2 - 3)}\Omega, \quad k > 0. \quad (73)$$

Unstable modes are present if $q > \sqrt{3} \simeq 1.732$, whereas the local Rayleigh criterion for instability is $q > 2$. Thus, the interplay between pressure and rotation present in boundary edge modes makes it possible for them to tap the free energy of differential rotation as a source of instability in a regime where local WKB modes cannot.

Note that the important case of Keplerian flow ($q = 1.5$) is stable. This is a consequence of the fact that the pressure gradient vanishes for this rotationally supported flow. Furthermore, it can be shown that the same type of calculation, applied to free shear flow (i.e. no Coriolis forces) produces *no* instabilities. Though normally a stabilizing influence, pressure gradients and rotation are destabilizing here. Tuning the right combination of rotation and pressure at the boundaries allows modes to extract angular momentum (and therefore energy) from the inner edge of the cylinder and transport it to the outer edge. In our simple example, it is a straightforward exercise to show that the unstable eigenmodes correspond to outward angular momentum transport, whereas the decaying eigenmodes correspond to inward transport.

We have worked this example through in some detail, because it is nicely illustrative of what is required for hydrodynamical instability driven by differential rotation. The mode is nonlocal, and depends upon radial wave trapping: in the case presented, the modes have nowhere to go but the edges. More complicated configurations, in which a region with large entropy gradients is embedded in a more uniform Keplerian disk, show similar unstable behavior (Lovelace et al. 1999, Li et al. 2000). Even when the local Rayleigh criterion is satisfied ($q < 2$), differential rotation can be destabilized when $q > \sqrt{3} = 1.732$. Communication between the different parts of the disturbance on either side of the corotation point ($x = 0$ in the example) is essential; it is easily shown that instability is not present when there is only one edge. The extraction of free energy from the differential rotation is a delicate matter depending on the phase correlation between the radial and azimuthal velocity fluctuations.

The role of Papaloizou-Pringle instabilities in astrophysical disks has yet to be established. It is likely to be of secondary importance in magnetized disks because of the MRI, but it is possible that there may be protostellar applications in regions where the disk gas is poorly coupled to the magnetic field. Even here, however, large departures from simple Keplerian profiles are required for instability, and it is not obvious that these are sustainable.

Global simulations of constant angular momentum tori (Hawley 1991) show that the nonlinear resolution of the Papaloizou-Pringle instability is not turbulence, but a spiral pressure wave. Moreover, the instability rapidly saturates when even a small amount of accretion is present (Blaes 1987). As a practical matter, the instability seems to be most important for nonmagnetized constant angular momentum tori, whereas Keplerian disks are more or less immune.

5 MHD Turbulence

5.1 Introduction

In elucidating the density wave theory of spiral structure, Lynden-Bell & Kalnajs (1972) posed a simple and revealing question: why should stellar disks be unhappy without spiral structure? The answer is that there are other configurations that share the same mass and angular momentum, but with less total energy. These correspond to a concentration of mass near the disk center, and a transference of angular momentum to large radial distances. The point is that in an asymptotic sense, all of the angular momentum can reside in none of the mass, and, even more importantly, bearing none of the *energy*. The hard part is to get the angular momentum out, which is precisely what a trailing density wave does.

The disruption of a differentially rotating flow into an accretion flow, the signature process of this review, occurs when (1) it is energetically favorable to do so; and (2) a path to these lower energy states is available. The lowering of disk energy must be accompanied by the outward transference of angular momentum, for this is the only route self-consistent with this objective. Recall that turbulence must be actively maintained, because it is highly dissipative: it needs access to a ready source of free energy. It is the end goal of minimized energy that makes the undertaking of this passage through turbulent flow worthwhile. The final outcome is a singular state with all the mass, shorn of its angular momentum, collected at the center of the potential well. An accretion disk is really nothing more than the sequence of intermediate states the gas is forced to pass through enroute to this final state.

There is a tradition, still ongoing, of assaulting Keplerian disks with a variety of instabilities taken from the fluid literature, hoping that one will take. Although many disk models are indeed vulnerable to one particular instability or another, this is generally because they have been so constructed. Only one process directly exploits the fact that an accretion disk is fundamentally unsatisfied in a state of Keplerian rotation: the magnetorotational instability. It is extraordinarily effective because magnetic fields are able to tap directly into the free energy sources of a fluid, the gradients of the flow that would be gone in an extremum energy state. It is of some interest to note that this is no less true of a *thermal* free energy source (temperature gradient) than of the rotational free energy source (angular velocity gradient) (Balbus 2001). The exquisite sensitivity to these free energy gradients imparted to a fluid by a magnetic field fundamentally alters the behavior of astrophysical gases in ways that hydrodynamical modeling cannot hope to capture. Viscous modelers beware.

5.2 The Magnetorotational Instability: A Simple Overview

The destabilizing role of a magnetic field in a differentially rotating fluid can be grasped with the aid of mechanical analogy. Imagine two nearby fluid elements displaced in the orbital plane from another by a spring-like force. Although nominally binding the elements together, the spring, if it is weak, will have exactly the opposite effect in a differentially rotating system. The element orbiting at smaller radius rotates more rapidly, and the spring torque lowers its angular momentum;

precisely the reverse happens for the element orbiting at larger radius, whose angular momentum is correspondingly increased. That must mean, however, that the small radius element drops down to yet smaller radii to accommodate its reduced angular momentum; conversely the large radius element moves to yet more distant radii. The spring tension grows with increasing element separation, and the process runs away. Note that angular momentum transport is not some non-linear consequence of the instability, it is the very cause of the (linear) instability. It flows, of course, outward.

It has been emphasized that the spring must be weak. Weak compared with what? The answer can be seen by noting our implicit use of circular orbit concepts in the above discussion. This is justified only if the natural oscillation frequency of the spring is less than the orbital frequency of fluid elements.

The simplest fluid system displaying this spring-like instability is an axisymmetric gas disk in the presence of a weak vertical magnetic field. The field has no effect on the disk equilibrium, which is a balance of gravitational and rotational forces. If a fluid element is displaced in the orbital plane by an amount $\boldsymbol{\xi}$, with spatial dependence e^{ikZ} , the induction (“field-freezing”) equation gives

$$\delta\mathbf{B} = ikB\boldsymbol{\xi}, \quad (74)$$

and the magnetic tension force is then

$$\frac{ikB}{4\pi\rho}\delta\mathbf{B} = -(\mathbf{k}\cdot\mathbf{v}_A)^2\boldsymbol{\xi}. \quad (75)$$

This is exactly the form of a spring-like force, linearly proportional to the displacement.

To follow the consequences of this force, we go into a frame of reference comoving with a small patch of the disk rotating at angular velocity $\Omega(R_0)$, where R_0 is our fiducial radius. We focus on a small radial neighborhood, so that $x = R - R_0$ is small in magnitude compared with R_0 . Terms of order $1/R$ are ignored, except $\Omega(R) = v_\phi/R$ which is our clock. (In this sense, v_ϕ is large.) In the corotating frame, Coriolis and centrifugal forces are present, and the difference between the centrifugal and gravitational forces is

$$R\Omega^2(R_0) - R\Omega^2(R) = -x\frac{d\Omega^2}{dR} \quad (76)$$

to leading order in x . The simplest case to examine is pressure-free displacements in the disk plane with a vertical wavenumber. With x and y respectively representing local radial and azimuthal displacements, the equations of motion then take on a very simple form

$$\ddot{x} - 2\Omega\dot{y} = -\left(\frac{d\Omega^2}{d\ln R} + (\mathbf{k}\cdot\mathbf{v}_A)^2\right)x \quad (77)$$

$$\ddot{y} + 2\Omega\dot{x} = -(\mathbf{k}\cdot\mathbf{v}_A)^2y. \quad (78)$$

These equations are in fact the rigorous leading order WKB equations for vertical wavenumber in a magnetized disk.

Equations (77) and (78) have solutions for x and y with time dependence $\exp(-i\omega t)$ provided that the dispersion relation

$$\omega^4 - \omega^2 \left[\kappa^2 + 2(\mathbf{k} \cdot \mathbf{v}_A)^2 \right] + (\mathbf{k} \cdot \mathbf{v}_A)^2 \left[(\mathbf{k} \cdot \mathbf{v}_A)^2 + \frac{d\Omega^2}{d \ln R} \right] = 0 \quad (79)$$

is satisfied. This is a simple quadratic equation for ω^2 , and it is straightforward to show that there are no unstable roots if and only if

$$\frac{d\Omega^2}{dR} \geq 0 \quad (80)$$

which replaces the Rayleigh stability criterion of outwardly increasing angular momentum (Balbus & Hawley 1991). The fastest growing mode has a growth rate of

$$|\omega_{max}| = \frac{1}{2} \left| \frac{d\Omega}{d \ln R} \right| \quad (81)$$

which occurs at a wave number given by

$$(\mathbf{k} \cdot \mathbf{v}_A)_{max}^2 = \left(\frac{1}{4} + \frac{\kappa^2}{16\Omega^2} \right) \left| \frac{d\Omega^2}{d \ln R} \right|. \quad (82)$$

Flows in violation of (80), which include most astrophysical cases of differential rotation, are prone to the magnetorotational instability.

Note that the maximum growth rate is, in the parlance of galactic structure, the local Oort-A value of the disk. Balbus & Hawley (1992) conjectured that this is the maximum growth rate that any local shearing instability can achieve in a disk, a result recently established for a rather general class of viscoelastic fluids (Ogilvie & Proctor 2003).

5.3 The Magnetorotational Instability: A Brief History

The understanding that the characteristic accretion disk combination of Keplerian rotation and a magnetic field is highly unstable emerged very belatedly, only a little more than a decade ago. Why this is so is an interesting question, given that disk stability research was already some 30 years old at the time, and modern accretion disk theory had been around for more than 20 years. The MRI calculation is not a difficult one, and work on the topic was initiated by no less a personage than Chandrasekhar (1953). How could such an important instability have been overlooked for so long? In fact, it wasn't. But neither was it well-understood.

The early studies by Chandrasekhar were extremely formal. Indeed, his 1953 paper was not at all astrophysical in context; it was a theoretical Couette flow analysis. Chandrasekhar limited his work on hydrodynamic and hydromagnetic stability to those configurations in which a *static* equilibrium could be defined and analyzed globally. But the lack of a coherent physical explanation of the instability hampered its understanding, making it difficult to perceive both its local character and widespread generality.

Recently proposed MRI laboratory experiments (Ji, Goodman, & Kageyama 2001; Noguchi et al. 2002; Rüdiger & Shalybkov 2002) have led to a detailed re-examination of Chandrasekhar's analysis of dissipative Couette flow, and rather

surprisingly, there appears to have been a rather straightforward oversight (Goodman & Ji 2002). Magnetized shear flow will of course draw out an azimuthal field from any radial component that happens to be present. In Chandrasekhar’s discussion, the term responsible for this behavior was dropped from the induction equation, on the grounds of a small magnetic Prandtl number approximation.² This was most unfortunate, because the process represented by this dropped term need not vanish in this limit; indeed, it is critical for the MRI to function.

How widespread this misapprehension became is difficult to say. (The error made its way into Chandrasekhar’s classic text [1961].) Much of the fluid and stellar community was aware of the instability, however, and its curious behavior of ostensibly changing the Rayleigh criterion discontinuously. Noteworthy studies include those of Velikhov (1959, the first derivation of a dissipationless angular velocity stability criterion for Couette profiles); Chandrasekhar (1960, a generalization of Velikhov’s result), Newcomb (1962, a variational approach); Fricke (1969, stellar differential rotation), Acheson & Hide (1972, geophysical applications); and Acheson & Gibbons (1978, more general stellar applications). But the robustness and the very general tendency of subthermal magnetic fields of *any* geometry to destabilize flows was never explicitly discussed. Indeed, the common wisdom was that magnetic fields were thought to be a stabilizing influence, and they were certainly a computational nuisance. It is telling that there are no references in the accretion disk literature to either Velikhov (1959) or Chandrasekhar (1960) prior to 1991.

The key conceptual point, which really has been grasped only in the last decade, is that *the limit $B \rightarrow 0$ retains the most salient behavioral features of a magnetized fluid*, and can be profitably investigated. One should think of an accretion disk not as a rotating fluid with a magnetic field, but as a magnetized fluid with rotation. By tethering fluid elements, magnetic fields impart *dynamical* significance to free energy gradients, which otherwise are felt only through their more ghostly diffusive presence. The stability properties of even a barely magnetized fluid are qualitatively different from those of a nonmagnetized fluid — a result which holds whether the fluid is rotating or not.

5.4 General Axisymmetric Stability Criteria

Convective and rotational instability are best handled simultaneously, since the affected mode is a joint buoyant-inertial disturbance. A rather general calculation is given by Balbus (2001), who considered the stability of a rotating, stratified plasma. The angular momentum and entropy distributions may be arbitrary functions of R and Z . With an eye toward applications involving hot dilute plasmas, a Coulomb thermal conductivity is assumed to be present. Heat is permitted to flow only along magnetic lines of force, a restriction which has important consequences. (Radiative conductivity, which would dominate in stellar interiors, gives rise to very different stability properties.) The flow is stable to axisymmetric disturbances provided that

$$-\frac{1}{\rho}(\nabla P) \cdot \nabla \ln T + \frac{\partial \Omega^2}{\partial \ln R} \geq 0, \quad (83)$$

²The magnetic Prandtl number is the dimensionless ratio of the viscous to resistive diffusivities.

$$\left(-\frac{\partial P}{\partial Z}\right) \left(\frac{\partial \Omega^2}{\partial R} \frac{\partial \ln T}{\partial Z} - \frac{\partial \Omega^2}{\partial Z} \frac{\partial \ln T}{\partial R}\right) \geq 0. \quad (84)$$

Note that the second inequality states that the angular velocity should increase outward along isothermal surfaces for stability. Without Coulomb conductivity, the stability conditions are

$$-\frac{3}{5\rho}(\nabla P) \cdot \nabla \ln P \rho^{-5/3} + \frac{\partial \Omega^2}{\partial \ln R} \geq 0, \quad (85)$$

$$\left(-\frac{\partial P}{\partial Z}\right) \left(\frac{\partial \Omega^2}{\partial R} \frac{\partial \ln P \rho^{-5/3}}{\partial Z} - \frac{\partial \Omega^2}{\partial Z} \frac{\partial \ln P \rho^{-5/3}}{\partial R}\right) \geq 0, \quad (86)$$

(Papaloizou & Szuszkiewicz 1992, Balbus 1995), whereas the classical hydrodynamical Høiland criteria are (Tassoul 1978)

$$-\frac{3}{5\rho}(\nabla P) \cdot \nabla \ln P \rho^{-5/3} + \frac{1}{R^3} \frac{\partial R^4 \Omega^2}{\partial R} \geq 0, \quad (87)$$

$$\left(-\frac{\partial P}{\partial Z}\right) \left(\frac{\partial R^4 \Omega^2}{\partial R} \frac{\partial \ln P \rho^{-5/3}}{\partial Z} - \frac{\partial R^4 \Omega^2}{\partial Z} \frac{\partial \ln P \rho^{-5/3}}{\partial R}\right) \geq 0. \quad (88)$$

Comparing these three sets of criteria, we see that the effect of a magnetic field is to replace gradients of conserved quantities in axisymmetric flow (angular momentum and entropy) with the free energy angular velocity and temperature gradients. The MRI is, in fact, only one manifestation of a very general principle. Magnetic torques ensure that angular velocity gradients are the stability discriminants for differentially rotating flow; magnetically confined conduction, when dominant, ensures that temperature gradients are the stability discriminants for a stratified gas.

5.5 Low-Ionization Disks

Our discussion has up to now implicitly assumed that the disk behaves completely hydrodynamically, or is fully magnetic. Here we focus on the transition from one behavior to the other.

A low-ionization gas contains at least three different fluids of interest: neutrals, ions, and electrons. Since, as we shall see, an astrophysical fluid typically becomes magnetically well-coupled at very small ionization fractions, the inertia resides in the neutrals, which couple collisionally to the ions more effectively than to the electrons. The electrons, on the other hand, bear the brunt of electrical current and so most closely correspond to the fluid associated with inductive field freezing. It is only an approximation to write the induction equation in terms of the bulk fluid velocity; more properly it is the electron velocity that should appear. The electrons are then coupled to the ions by self-induction, whereas the ions are coupled to the neutrals via collisions.

In a fully-magnetized fluid, all of these couplings are strong. More generally, the electron fluid velocity \mathbf{v}_e may be rewritten

$$\mathbf{v}_e = \mathbf{v} + (\mathbf{v}_e - \mathbf{v}_i) + (\mathbf{v}_i - \mathbf{v}) \quad (89)$$

where \mathbf{v} is the velocity of the dominant neutrals, and \mathbf{v}_i the ion velocity. The electron-ion velocity difference is just proportional to the current, and leads to Hall electromotive forces in the induction equation (e.g. Wardle & Königl 1993). The ion-neutral difference is related to ambipolar diffusion, and is proportional to the Lorentz force (Shu 1992). The resulting full induction equation is a bit daunting, but Balbus & Terquem (2001) give useful order-of-magnitude scalings for the relative importance of each of the terms that appear. One important and often overlooked conclusion is that in astrophysical settings, the Hall electromotive force is at least as important as ohmic dissipation, and can be destabilizing (Wardle 1999; Balbus & Terquem 2001).

In protostellar disks, an ionization fraction as small as 10^{-13} can start to induce magnetic coupling on AU scales. However, even this level may not be attainable in a dusty disk where grains are the dominant charge carriers (Umebayashi & Nakano 1988). To add to the uncertainty, T Tauri systems are X-ray sources (Glassgold, Feigelson, & Montmerle 2000; Fromang, Terquem, & Balbus 2002), which introduces a potent time-varying ionization source. The role of cosmic rays, another potential ionization source, in maintaining the MRI in the outer disk layers has been examined by Gammie (1996).

The magnetic behavior of protostellar disks is extremely uncertain, largely because neither the disposition of the dust nor the chemical properties of the gas are well understood. It seems likely that there will be evolutionary phases when only the most distant (low density) and innermost (hot) gas will be magnetized, but it is also possible that an active X-ray source and agglomerated dust grains may render much of the disk magnetically well-coupled (Fromang et al. 2002).

Protostellar disks are not the only astrophysical venue where these issues arise. The outer regions of CV disks (and possibly other close binary disks) also appear to be in the low-ionization regime (Gammie & Menou 1998). It has been suggested that Hall electromotive forces may be of some relevance to understanding the “low state” of such systems (Balbus 2002). In these objects, dust grain physics is less likely to be an important complication than it is for protostellar disks. The magnetic coupling properties of cool AGN disks are discussed by Menou & Quataert (2001).

5.6 *Turbulent Transport in Thin Disks*

Differentially rotating disks, in particular Keplerian disks, are unstable in the presence of a magnetic field to the MRI, which transports angular momentum outward even in the linear stages of the instability. Although the disk could alleviate its difficulties by heading toward a state of uniform rotation, this is not what happens. Rather, the excess angular momentum acquired by the outer regions instead allows them to occupy even more remote orbits where they rotate yet more slowly. Correspondingly, the inner disk regions that have lost angular momentum slide into lower lying orbits, and rotate yet more rapidly. Far from eliminating outwardly decreasing angular velocity gradients, the disk instead behaves in such a way as to accentuate such “unfavorable” rotation profiles. The ensuing nonlinear turbulence is compatible with this linear angular momentum segregation: energy is lost via turbulent dissipation, and the global minimum energy state corresponds to a mass concentration at the dynamical center and all

the angular momentum dispersed to infinity. The dispersed angular momentum need not, as a matter of principle, have finite mass or finite energy associated with it. The disk's struggle to attain this singular energy minimum is the topic of this section.

5.6.1 Classical Viscous Disk Theory

Traditionally, anomalous (read “turbulent”) disk transport has been modeled as an enhanced Navier-Stokes viscosity, a technique developed by Lynden-Bell & Pringle (1974) that illustrated certain key energetic and evolutionary processes. The approach was never meant to embody the dynamics of accretion disk turbulence, a very important qualification all too often lost in subsequent applications of the theory. To understand how MHD turbulent transport is related to features of viscous disk theory, begin with the viscous stress tensor, which is assumed to be dominated by its $R\phi$ component

$$\sigma_{R\phi} = \nu\rho \frac{d\Omega}{d \ln R}, \quad (90)$$

where ν is the (turbulent) viscous shear diffusivity. The height integrated equations of mass and angular momentum conservation are

$$\frac{\partial \Sigma}{\partial t} + \frac{1}{R} \frac{\partial R \Sigma v_R}{\partial R} = 0, \quad (91)$$

and

$$\frac{\partial}{\partial t}(\Sigma R^2 \Omega) + \frac{1}{R} \frac{\partial}{\partial R}(\Sigma R^3 \Omega v_R - \nu \Sigma R^3 \frac{d\Omega}{dR}) = 0, \quad (92)$$

where Σ is the integrated disk column density.

Under steady state conditions, the mass flux

$$\dot{M} \equiv -2\pi R \Sigma v_R$$

and the angular momentum flux must both be constant. Assuming that the viscous stress vanishes at the inner edge of the disk R_0 leads to

$$\dot{M} \left[1 - \left(\frac{R_0}{R} \right)^{1/2} \right] = 3\pi\nu\Sigma. \quad (93)$$

This completely determined the functional form of the turbulent viscosity parameter $\nu\Sigma$, which can now be eliminated in favor of the more accessible quantity \dot{M} . In particular, ν thermalizes the free energy of differential rotation at a rate per unit area given by

$$Q_e = \frac{\nu\Sigma}{2} \left(\frac{d\Omega}{d \ln R} \right)^2 = \frac{9}{8} \nu \Sigma \Omega^2. \quad (94)$$

Eliminating ν then gives

$$Q_e = \frac{3GM\dot{M}}{8\pi R^3} \left(1 - \left(\frac{R_0}{R} \right)^{1/2} \right), \quad (95)$$

the classical (Q_e, \dot{M}) relationship (Lynden-Bell & Pringle 1974). The additional assumption that the heating is radiated locally by a thermal surface flux σT_{eff}^4

then leads to a surface profile $T_{eff}(R) \propto R^{-3/4}$, and, it can be shown, a characteristic $\nu^{1/3}$ spectral flux profile (Lynden-Bell 1969). At this point, however, the theorist's luck runs out: except for the occasional cooperative CV system (Frank, King, & Raine 2002), real accretion disks have considerably more complex spectra that are not well-understood (e.g. Blaes 2002). Nevertheless, equation (95) with Q_e determined observationally, is the cornerstone relation of disk phenomenology, and is widely used to deduce mass accretion rates. It has the advantage of being independent of the viscosity parameter, which suggests a validity that extends beyond viscous disk models.

A time-dependent equation for the evolution of Σ emerges by combining equations (91) and (92):

$$\frac{\partial \Sigma}{\partial t} = \frac{3}{R} \frac{\partial}{\partial R} \left[R^{1/2} \frac{\partial}{\partial R} (\nu R^{1/2} \Sigma) \right] \quad (96)$$

This diffusion-like equation is commonly used in accretion disk modeling, but requires an *a priori* specification of ν to be implemented. Nevertheless, it shows explicitly how disks evolve to their singular end state of mass concentration at the origin and angular momentum dispersal to infinity.

5.6.2 MHD Turbulent Transport in Thin, Radiative Disks

The relationship between the phenomenological disk theory of the previous section and MHD turbulence has been investigated using a simple statistical approach (Balbus & Papaloizou 1999). The idea is to separate the Keplerian rotation profile from the net velocity vector, and focus on the residual velocity \mathbf{u}

$$\mathbf{v} = R\Omega \hat{\mathbf{e}}_\phi + \mathbf{u}. \quad (97)$$

We assume that the mean accretion drift velocity is small compared with fluctuation amplitudes. The hierarchy is

$$|\langle \mathbf{u} \rangle|^2 \ll \langle u^2 \rangle \ll R^2 \Omega^2. \quad (98)$$

A key assumption is that since the disk is thin, we may average fluctuating quantities over a radial distance ΔR , large compared with a vertical scale-height H , but small compared with R , and thereby formulate a ‘‘local’’ disk theory. (This is sensible only if $H/R \ll 1$, otherwise a time or ensemble average must be used.) The theory is thus expressed in terms of evolutionary PDEs in R and t , and the dynamical fluid quantities have been vertically integrated and azimuthally averaged, and weighted by density:

$$\langle X \rangle = \frac{1}{2\pi \Sigma \Delta R} \int_{-\infty}^{\infty} \int_{R-\Delta R/2}^{R+\Delta R/2} \int_0^{2\pi} \rho X \, d\phi \, dR \, dz, \quad H \ll \Delta R \ll R, \quad (99)$$

where now Σ must itself be defined as a height-integrated, azimuthally and radially averaged quantity. Mass and angular momentum conservation then follow from our equations (1) and (5):

$$\frac{\partial \Sigma}{\partial t} + \frac{1}{R} \frac{\partial (R \Sigma \langle u_R \rangle)}{\partial R} = 0 \quad (100)$$

$$R^2\Omega\frac{\partial\Sigma}{\partial t} + \frac{1}{R}\frac{\partial}{\partial R}\left(R^3\Omega\Sigma\langle u_R\rangle + R^2\Sigma W_{R\phi}\right) = 0 \quad (101)$$

where $\Sigma W_{R\phi}$ is obtained from $T_{R\phi}$ after height integration and averaging. Since $W_{R\phi}$ has dimensions of velocity squared, it is convenient to normalize this quantity to the isothermal sound speed $c_S^2 = P/\rho$. Depending on the problem of interest, the value of c_S^2 chosen for normalization might be local, or it could be a suitably defined global average. The ratio α is then a measure of the strength of the turbulent angular momentum transport (Shakura & Sunyaev 1973):

$$\alpha c_S^2 \equiv W_{R\phi}. \quad (102)$$

For MHD turbulence, α is an indication of the amplitude of rms turbulent fluctuations, but this need not be generally true: it depends upon the existence of a good positive correlation between the R and ϕ components of the stress tensor. In analytic modeling α is generally assumed to be constant, but there is no compelling justification for this, and numerical simulations show a highly complex spatio-temporal structure for α (Nelson & Papaloizou 2003).

Equations (100) and (101) lead to an evolutionary relation between Σ and $W_{R\phi}$ (Balbus & Papaloizou 1999):

$$\frac{\partial\Sigma}{\partial t} = \frac{1}{R}\frac{\partial}{\partial R}\left[\frac{1}{(R^2\Omega)'}\frac{\partial}{\partial R}(\Sigma R^2 W_{R\phi})\right], \quad (103)$$

where the prime $'$ indicates d/dR . Diffusive evolution is therefore not a unique consequence of adopting a viscous stress model. It follows instead from mass and angular momentum conservation in a Rayleigh-stable disk, and the notion of coarse grain averaging implicit in the assumption that $W_{R\phi}$ exists.

5.6.3 Thin Disk Energetics

Consideration of the disk energetics comprises the other key step in recovering viscous disk theory. The dominant terms in the energy flux appear to be

$$\left(\frac{1}{2}R^2\Omega^2 + \Phi\right)\Sigma\langle u_R\rangle + \Sigma R\Omega W_{R\phi}. \quad (104)$$

This places a powerful constraint upon thin disk models, since energy transport introduces no new turbulent correlations into the equations of motion beyond $W_{R\phi}$. The point is that $\langle u_R\rangle$ and $W_{R\phi}$ are tightly restricted by the demands of mass and angular momentum conservation. In particular, one is not at liberty to demand that the total mechanical energy of the fluctuations plus “background disk” be conserved. Balbus & Papaloizou (1999) show for both evolving and steady disks that the mechanical energy loss is in fact

$$Q_e = -\Sigma W_{R\phi}\frac{d\Omega}{d\ln R}. \quad (105)$$

This expression represents true radiative energy losses in a thin disk. Note, however, that the right hand side is the rate at which free energy is extracted from the large-scale differential rotation, and is not, itself, a dissipative quantity (see §3.3). Self-consistent thin disk theory imposes the very stringent requirement that *all* of this energy be radiated locally. Non-radiative flows, which are characterized by $c_S \sim R\Omega$, behave differently.

5.7 *Transport in Low Radiation Accretion Flows*

Accretion sources in nature show far more variety than the rather tightly constrained Keplerian thin disk model is capable of, and theorists have for some time been exploring the behavior of accretion in which radiative losses play a subdominant role (e.g., Ichimaru 1977; Begelman 1978; Abramowicz et al. 1988). Interest in these solutions rapidly grew in the mid-90's when a series of seminal papers appeared (Narayan & Yi 1994, 1995) with the goals of constructing simple one-dimensional models of these accretion profiles and elucidating their signature observational properties (Narayan, Mahadevan, & Quataert 1998 for a review). The recent unambiguous Chandra detection of the highly subluminal Galactic Center source Sgr A* in X-rays (Baganoff et al. 2001) furnishes compelling evidence that “dark accretion” exists in some guise, and poses a well-defined theoretical challenge (Narayan 2002).

Unlike the case of radiative Keplerian accretion disks, in which there is at least agreement on the basics of the behavior of simple models, there is no broad consensus on the dynamical properties of low radiation accretion flows. The Sgr A* detection has made one initially controversial suggestion — that electrons in such flows are cooler than the ions (Narayan & Yi 1995) — increasingly hard to avoid. Yet the following questions continued to be argued in the literature: Are these flows marked predominantly by inward or outward energy transport? Are they quasi-spherical? Do their rotation profiles differ markedly from Keplerian? Can they be dominated by thermal convection? It has even been suggested that in the presence of thermal convection, the turbulent rotating accretion flow is characterized by a vanishing stress tensor $T_{R\phi}$ and by vanishing dissipation (Narayan, Igumenshev, & Abramowicz 2000; Abramowicz et al. 2002), though these arguments have been criticized on both energetic and thermodynamic grounds (Balbus & Hawley 2002; Narayan et al. 2002 for a response).

Steady bulk accretion is a far from obvious outcome in a gaseous system which is marginally bound to start with, and subsequently stirred by the free energy of differential rotation (Pringle & Rees 1972), a point that has recently been revisited anew (Blandford & Begelman 1999). As in thin disks, nonradiating gas gradually loses rotational support, but unlike the radiative models, here it retains a significant level of thermal support. In fact, even in the absence of any rotation, spherical (Bondi) accretion is not possible if the adiabatic index exceeds 5/3, as it effectively does in a heated, nonradiative gas. It is thus hardly surprising that in numerical MHD simulations most of the mass is lost not down the hole, but through the outer boundaries of the computational grid (Hawley & Balbus 2002).

A local viscous prescription for angular momentum transport, which as we have seen is well-motivated for a rotationally thin disk (see §5.6.2), breaks down completely for a non-radiative flow. This is a nuisance for the theorist, but it is inescapable. Not only is there no longer a clean separation of turbulent and global scales, there are other turbulent correlations that appear in the transport equations which are not part of the $T_{R\phi}$ stress tensor. The most important of these is the correlation in velocity and temperature fluctuations seen in equation (49). These have no counterparts in *viscous* energy transport, but are in fact much more closely analogous to the wave energy fluxes of §3.

The MRI is the fundamental instability that converts differential rotation into

turbulent fluid motions, whether the system is radiative or not. Inward accretion does lead to the development of adverse entropy gradients however (Narayan & Yi 1994), which are often then credited with giving rise to a “second” instability. In fact, the generalized Høiland criteria (e.g. eqs. [83], [84]) show that these are really secondary features of the same instability. (Note that in the presence of thermal conduction, an outwardly decreasing temperature profile is likely to be destabilizing.) But no secondary adverse thermal gradient can cause the stress tensor $T_{R\phi}$ to vanish or to change sign in an accretion flow driven by the MRI: a positive stress is intimately linked to the flow of free energy from the differential rotation to the turbulent fluctuations.

Despite the enormous output of analytical and quasi-analytical treatments in the literature, the global behavior of nonradiative, differentially rotating accretion flows is almost certainly too complex to capture by standard viscous modeling. Numerical simulations hold some promise of telling us, if not everything, then at least where the matter goes.

6 Numerical Simulations of MHD Disk Turbulence

6.1 The Local Approximation

6.1.1 Equations and Boundary Conditions

While attempts are occasionally made at phenomenological theories of turbulent flow, numerical study has proven to be extremely fruitful. Both analytic and numerical approaches must each make compromises, and remain limited in scope. The principal advantage of numerics is that brute strength is useful! The increase in raw computational power in the last decade has been phenomenal, and simulations of true three-dimensional turbulence are now a reality.

In the study of accretion disks, two computational schemes are generally used, local and global. Global simulations, which are more difficult, are discussed in section 7. In the *local approximation*, the idea is to focus on a small region of the disk, forcing the new origin to corotate with disk fluid orbiting at a particular angular velocity, Ω_0 . All velocities are measured relative to $R\Omega_0$. In the local limit, curvature terms are ignored. More formally, the asymptotic regime is defined by

$$R \rightarrow \infty, \quad v_\phi \rightarrow \infty, \quad \frac{v_\phi}{R} = \Omega \rightarrow \text{finite}. \quad (106)$$

We define the velocity \mathbf{w} :

$$\mathbf{w} = \mathbf{v} - R\Omega_0 \mathbf{e}_\phi. \quad (107)$$

The value of R at which $\Omega = \Omega_0$ will be denoted R_0 . In general we shall consider only small radial excursions from R_0 ,

$$R = R_0 + X, \quad X \ll R_0. \quad (108)$$

Thus,

$$R\Omega_0^2 - \frac{\partial\Phi}{\partial R} = R(\Omega_0^2 - \Omega^2(R)) \simeq -X \left. \frac{d\Omega^2}{d\ln R} \right|_{R=R_0} \quad (109)$$

to leading order. Local Cartesian coordinates can be defined by aligning the X and Y axes along R and ϕ . In a frame rotating at Ω (dropping the subscript), the local equations of motion for w_X and w_Y are

$$\frac{\partial w_X}{\partial t} + \mathbf{w} \cdot \nabla w_X - 2\Omega w_Y + X \frac{d\Omega^2}{d \ln R} = -\frac{1}{\rho} \frac{\partial P_{tot}}{\partial X} + \frac{\mathbf{B}}{4\pi} \cdot \nabla B_X \quad (110)$$

$$\frac{\partial w_Y}{\partial t} + \mathbf{w} \cdot \nabla w_Y + 2\Omega w_X = -\frac{1}{\rho} \frac{\partial P_{tot}}{\partial Y} + \frac{\mathbf{B}}{4\pi} \cdot \nabla B_Y \quad (111)$$

where P_{tot} is the gas plus magnetic pressure. The forms of the remaining dynamical equations remain unaffected by the change to rotating coordinates.

Extended three-dimensional simulations require what are known as shearing-box boundary conditions. In this approach, the azimuthal boundary conditions are always periodic. Vertical boundary conditions may be either periodic or outflowing, depending upon the problem of interest. Because of the presence of large-scale shear, the radial boundary conditions require more care to specify (Hawley, Gammie, & Balbus 1995). They are quasi-periodic: the computational domain is thought of as one brick in a brick wall extending to infinity, each brick with the same internal fluid configuration as the next. The velocity shear is uniform across the entire brick wall, so one layer of bricks slides with respect to the layer above and below! A fluid element leaving a radial boundary of the one-brick computational domain is replaced by its image on the opposite side, but not, in general, at the azimuth it has just vacated. Rather, the image reappears at the azimuth of the sliding brick that the original fluid element is entering. The mathematical formulation of these boundary conditions may be found in Balbus & Hawley (1998).

6.1.2 Local Two-Dimensional Simulations

In the first extended axisymmetric simulations carried out by Hawley & Balbus (1992), a surprise emerged. Though the evolution of an initial uniform vertical magnetic field was in accord with analytic theory in the linear stages of its development, the nonlinear stages did not appear to be turbulent at all. In fact, the linear stage seemed to continue indefinitely, with exponentially growing streaming motions persisting. This contrasted sharply with the nonlinear behavior of a shearing box starting with a vertical field whose mean value was zero—half upwards and half downwards say, or sinusoidally varying. In that case, turbulence quickly developed after a few linear growth times, and then gradually decayed, leaving no field at all at the end of the simulation.

The latter behavior is a consequence of Cowlings' anti-dynamo theorem (e.g. Moffatt 1978), which prohibits field amplification in an isolated axisymmetric MHD flow. The case of a mean vertical field avoids this restriction because it does not meet the requirement of isolation: the field extends to infinity. This is not necessarily unphysical: real disks certainly can be threaded by a magnetic field which closes at very large distances away from the midplane. The question is, do such disks exhibit the streaming behavior discussed above in three-dimensions?

6.1.3 Local Three-Dimensional Simulations

The study of true dynamo amplification requires the implementation of three-dimensional MHD codes. The simplest approach consists of a homogeneous shearing box, in which only the radial component of the large-scale gravitational field is retained (Hawley et al. 1995; Matsumoto & Tajima 1995). The initial field geometry in these studies had some combination of vertical and toroidal components. A more complicated initial field configuration, important for investigating dynamo activity, is to give the initial field a random character with vanishing mean value (Hawley, Gammie, & Balbus 1996). Finally, adding a vertical component of the gravitational field produces a density stratification (Brandenburg et al. 1995; Stone et al. 1996), and introduces buoyancy into the problem.

The answer to the question posed at the end of the previous subsection is that three-dimensional studies in fact do show the breakdown of the two-dimensional streaming solutions (Hawley et al. 1995). If the computational box is large enough to allow an unstable radial wavelength, streaming is disrupted within a few orbits, as the Kelvin-Helmholtz instability noted by Goodman & Xu (1994) leads to fluid turbulence, and of course its large associated angular momentum transport.

Later work by Stone et al. (1996) introduced vertical stratification, allowing for two vertical scale-heights in an initially isothermal disk. With the onset of the MRI, the magnetic field emerged from the disk to establish a highly magnetized corona. However, the amplitude of the turbulence near the midplane is determined more by local dissipation than by buoyant losses, and the resulting stress and transport levels are not greatly modified from the nonstratified simulations. The presence of a corona, however, may well have important observational consequences, especially if a significant amount of dissipational heating occurs there. Miller & Stone (2000) performed simulations with a larger computational domain covering 5 scale heights above and below the equator. They showed that a strongly magnetized corona ($P_{\text{gas}} \ll P_{\text{mag}}$) forms rather naturally from little more than a disk and a weak seed field.

6.2 Radiative Effects

The radiation energy density in the inner regions of black hole accretion rivals or exceeds the thermal energy density. The linear stability of a magnetized, stratified, radiative gas was recently addressed by Blaes & Socrates (2001). Despite the complexity of the full problem, the MRI emerges at the end of the day unscathed, its classical stability criterion $d\Omega^2/dR > 0$ remaining intact. The maximum growth rate can be lowered, however, when the azimuthal field approaches or exceeds thermal strength. (The same is true for the ordinary MRI, as shown by Blaes & Balbus [1994].)

The proper interpretation of a linear analysis is slightly unclear, since the unperturbed state is presumably fully turbulent due to the MRI; a rotationally stable disk lacks an internal energy source. The interplay between MHD turbulence and radiation is intrinsically nonlinear. Turner, Stone, & Sano (2002), have studied a local, radiative, axisymmetric, shearing box. The linear calculations of Blaes & Socrates (2001) were confirmed in detail, and the nonlinear flow fully developed. As in standard MRI simulations, the stress is dominated by the Maxwell

component, which is a factor of a few larger than the Reynolds terms. Photon diffusion maintains nearly isothermal conditions while creating over-dense small clumps of thermally-supported gas. This occurs when radiation pressure support is rapidly lost via small wavelength diffusion. Optically thick radiative disks may therefore be more inhomogeneous than their gaseous counterparts.

6.3 Low Ionization Disk Simulations

Protostellar disks, and possibly cataclysmic variable disks, contain regions of low ionization fraction—so low that the assumptions of ideal MHD break down. Ohmic dissipation becomes important, together with the Hall inductive terms. The effects of Hall electromotive forces on the MRI have been studied by Wardle (1999) and by Balbus & Terquem (2001). Nonlinear numerical simulations including ohmic resistivity have been done by Fleming, Stone, & Hawley (2000); Sano & Stone (2002) have done simulations including both the ohmic and Hall processes. Under rather general conditions, if Ohmic dissipation is important, Hall electromotive forces are also important (Balbus & Terquem 2001; Sano & Stone 2002).

The most interesting feature introduced by Hall electromotive forces is helicity: the relative orientation of the angular velocity $\boldsymbol{\Omega}$ and magnetic field \boldsymbol{B} vectors matters (Wardle 1999; Balbus & Terquem 2001). The key point is that $\boldsymbol{\Omega} \cdot \boldsymbol{B} > 0$ configurations raise the maximum growth rate in the presence of ohmic losses, and this aligned configuration results in more vigorous transport in the local axisymmetric simulations of Sano & Stone (2002). In configurations where $\boldsymbol{\Omega} \cdot \boldsymbol{B}$ vanishes on average, the level of turbulence is much more sensitive to the size of the ohmic dissipation term.

In the simulations of Fleming et al. (2000), a critical magnetic Reynolds number Re_M emerged below which turbulence is suppressed. (Re_M is defined here as the ratio of the product of the scale height and sound speed to the resistivity.) When the mean field vanishes, Re_M was found to be surprisingly high, $\sim 10^4$. In the presence of a mean field, the critical $Re_M \sim 10^2$. The interesting and important question is whether the inclusion of Hall electromotive forces changes these numbers by lowering them, i.e., making it easier to support turbulence. The Sano & Stone (2002) axisymmetric simulations did not reveal a large change, but questions on the maintenance of turbulence more properly await a three-dimensional treatment.

7 Global Disk Simulations

Global accretion simulations are a demanding computational problem, requiring extended evolution at high resolution. Resolving the turbulent cascade through its full inertial range is not yet possible. The global disk structure alone extends from the black hole horizon, r_S , out to $\sim 10^3 r_S$. Time scales $\propto \Omega$, so that Keplerian rotation implies a factor of $\sim 3 \times 10^4$ in time scales. While compromises are unavoidable, the problems of interest are so rich that much can be learned even from highly idealized flows.

7.1 Two-Dimensional Simulations

Given the difficulties of these simulations, it is somewhat surprising to note that global axisymmetric MHD disk studies have been around for almost two decades, largely motivated by jet formation problems (Uchida & Shibata 1985). It is only more recently that two-dimensional simulations have focused on the internal dynamics of the disk itself and the resulting accretion flow, rather than on the launching and collimation of jets.

The challenge of understanding under-luminous accreting compact objects has been, from the numericist’s perspective, a most welcome development. This is precisely the type of flow that is well-suited to numerical simulation. The first two-dimensional MHD simulations of nonradiating accretion flows were carried out by Stone & Pringle (2001). In this study, accretion begins from a constant angular momentum torus, with weak embedded poloidal field loops. The initial infall phase is relatively smooth, and marked by streaming. Subsequent evolution is decidedly turbulent. The resulting flow consists of an approximately barotropic disk near the midplane, with constant Ω contours parallel to cylindrical radii. A substantial magnetized coronal outflow enveloped the disk. Finally, there was very little difference in the character of the solution if dissipative losses were retained as heat or simply ignored.

Toward the end of the Stone & Pringle (2001) simulations, the turbulence is noticeably waning, because there is nothing to save it from the anti-dynamo theorem. Axisymmetric simulations also tend to over-emphasize radial streaming, and cannot allow for toroidal field instabilities. Notwithstanding these limitations, by allowing a rapid investigative turnover of plausible accretion scenarios, two-dimensional simulations have proven to be a valuable tool, and a remarkably reliable one as well.

7.2 Cylindrical Disks

The “cylindrical disk” is a global three-dimensional system allowing for full radial and azimuthal dynamics, but ignoring the vertical component of the central gravitational field. Although there is no vertical stratification, turbulence and magnetic fields can be sustained with far fewer vertical grid zones than required for a full three-dimensional simulation.

Armitage (1998) carried out the first such calculation using the standard ZEUS code and a grid covering the full 2π in azimuth, running from $R = 1$ to 4, and $Z = 0$ to 0.8. The radial boundaries were reflecting, the vertical boundaries periodic. The initially vertical magnetic field was taken proportional to $\sin(kR)/R$, with the sine function argument varying over 2π between $R = 1.5$ and 3.5. MHD turbulence rapidly developed.

A more extensive set of cylindrical simulations (Hawley 2001) reaffirmed many of the conclusions of the local box models, and tested several technical aspects of global simulations. Restricting the azimuthal range to some fraction of 2π does not seem to affect the qualitative outcome of a simulation, nor does the polytropic index in the equation of state. Simulations that start with a vertical field, however, have greater amplification and higher ratios of stress to magnetic

pressure compared with those beginning with toroidal fields.

Cylindrical disk calculations have been applied to the problem of the star-disk boundary layer (Armitage 2002; Steinacker & Papaloizou 2002). Such simulations clearly represent an important step forward beyond viscous models. Both sets of investigators reported dynamo amplification. In particular, Armitage (2002) finds an order of magnitude larger field energy density in the boundary layer compared with the average disk field. Dissipative heating in the boundary layer has yet to be simulated.

7.3 *Three-Dimensional Simulations*

Global three-dimensional MHD disk simulations with complete vertical structure have been discussed by Hawley (2000). Here, the initial configuration is a constant angular momentum tori with a weak embedded magnetic field, which could be either toroidal or poloidal. Such structures appear in models of active galactic nuclei, where it is thought that they feed an inner disk (Krolik 1999). But the most notable feature of Hawley’s simulations is the speed with which an initial constant angular momentum profile is changed to nearly Keplerian—a few orbital times at the pressure maximum of the initial torus. The weak field instability is so efficient at transporting angular momentum, that vigorous radial spreading dilutes the structural pressure gradient, leaving the disk rotationally supported. At later times in the course of the simulation, the disks show strong time and space variability on all resolvable scales, and tightly wrapped spiral structure. There is significant angular momentum transport: typical α values are several percent, with pronounced and rapid fluctuations. Similar results were obtained (for toroidal fields) by Machida, Hayashi, & Matsumoto (2000).

Steinacker & Henning (2001) revisit the question of the influence of a large-scale vertical field on an accretion disk, previously studied in axisymmetry. They obtain very high accretion rates, which is described as a “collapse.” Coupling of the disk to a magnetized corona also appears to drive outflows, with the degree of collimation depending on the strength of the field.

Hawley & Krolik (2001, 2002) investigate the evolution of a magnetized accretion torus lying near the marginally stable orbit in a pseudo-Newtonian model potential for the black hole (Paczynski & Wiita 1980). These papers focus on the behavior of the stress tensor in gas passing through the so-called plunging region inside of the marginally stable circular orbit. In contrast to standard viscous models, the simulations suggest that the disk does not sharply truncate at the marginally stable orbit, nor does the stress vanish here. (The stress actually increases somewhat in the plunging region, owing to the strong correlation engendered in the radial and azimuthal field components.) Once again, variability is seen over a large range of spatial and time scales.

The more general problem of nonradiative global accretion over larger radial domains, first considered in two dimensions by Stone & Pringle (2001), has been extended to three dimensions by Hawley, Balbus & Stone (2001) and Hawley & Balbus (2002). Once again the accretion originates with a constant specific angular momentum torus. But in these simulations, the torus is initially centered out rather far out, at 100 Schwarzschild radii from the hole. The resulting turbulent

flow appears at the end of the simulation to settle into three well-defined dynamical structures. What accretion is present is via a hot, thick, slightly sub-Keplerian disk, which evidently is characteristic of radiative and nonradiative disks alike. Surrounding this disk is a strongly magnetized corona with vigorous circulation and perhaps a weak outflow. Magnetic coronal pressure confines a jet-like outflow, pinning it against the centrifugal funnel wall, an effective equipotential surface.

Figure (2) shows schematically the appearance of the disk, corona, and jet as they appear in a typical run. The inner torus is pressure-thickened, but remains predominately supported by rotation. It is a transitory structure, forming and collapsing over the course of the simulation.

8 Summary

Our understanding of the basis of astrophysical accretion has deepened enormously in the past decade, and the physical process underlying the “anomalous viscosity” of accretion disks has been elucidated. I believe that the term itself should be avoided, since it is so misleading. Magnetic fields do much more than fill the role occupied by a hydrodynamical Navier-Stokes viscosity. The behavior of magnetized fluids is far too subtle for this approach to be profitably carried into its fourth decade.

A one sentence summary of the effects of weak magnetic fields on the stability of a gaseous system is as follows: Magnetic fields turn gradient free energy sources (angular velocity and temperature) into sources of dynamical instability. Provided the assumptions inherent in the MHD approximation remain valid, the fields maintain this influence even in the formal limit $B \rightarrow 0$. This is why any formal stability analysis on an *ersatz* viscous gas is likely to be misleading, at best.

The combination of a magnetic field and outwardly decreasing differential rotation is thus prone to what is generally known as the magnetorotational instability, or MRI for short. Localized simulations of Keplerian disks indicate that the MRI leads to a turbulence-enhanced stress tensor that transports energy and angular momentum outwards, allowing accretion to proceed. The typical dimensionless value of the stress (normalized to a fiducial pressure) ranges from 5×10^{-3} to 0.6 depending upon field geometry, and is highly variable in both space and time. Local simulations have become rather sophisticated in the range of problems they are able to address, and work has now begun to include radiation dynamics and non-ideal MHD. There is still considerable uncertainty of how magnetic fields behave in disks containing regions of low ionization, and hydrodynamical processes certainly cannot be ruled out. Wave transport, of interest in its own right as well as for the perspective it brings to turbulent transport, is likely to be central to our understanding of protoplanetary disk evolution. Studies of the interaction between density waves and MHD turbulence have barely begun.

Global three-dimensional MHD simulations are now being run by several groups of investigators. The most robust finding of these studies is the speed with which a Keplerian profile emerges from an initial thick torus configuration, whatever the field geometry. The most detailed simulation performed to date (Hawley & Balbus 2002) ends in a three component structure: a warm Keplerian disk, a

highly magnetized corona, and an axial jet. Considerably more exploration needs to be done before we can be certain of whether this outcome is generic.

The unique spatial resolution and sensitivity capabilities of the Chandra X-ray satellite provide an auspicious opportunity to bridge the gap between computational gas dynamics and observed spectra. Chandra observations of the Galactic Center provide compelling evidence that very low luminosity accretion flows are present in nature, and these the numericist may hope to simulate with perhaps some fidelity. Relatively little has been done to elicit the radiative properties of the vast digital accretion flow data base. There are grounds for some hope that this untapped resource may advance our understanding of black hole accretion as much as has the last remarkable decade.

Acknowledgements

It is a pleasure to thank S. Fromang, J. Hawley, and K. Menou for reading an early version of this review. All made constructive comments that greatly improved the presentation. Support under NSF grant AST-0070979, and NASA grants NAG5-9266 and NAG-10655 is gratefully acknowledged.

References

- Abramowicz, M. A., Czerny, B., Lasota, J. P., & Szuszkiewicz, E. 1988. *Ap. J.* 332:646–58
- Abramowicz, M. A., Igumenshev, I. V., Quataert, E., & Narayan, R. 2002, *ApJ*, 565, 1101
- Acheson, D. J., & Gibbons, M. P. 1978. *Philosophical Transactions of the Royal Society of Londn. Series A, Mathematical and Physical Sciences.* 289, 1363:459–500
- Acheson, D. J., & Hide, R. 1972. *Rep. Prog. Phys.* 36:159–221
- Armitage, P. J. 1998. *Ap. J.* 501:L189–92
- Armitage, P. J. 2002. *MNRAS* 330:895–900
- Baganoff, F. K., Bautz, M. W., Brandt, W. N., Chartas, G., Feigelson, E. D., Garmire, G., Maeda, Y., Morris, M., Ricker, G. R., Townsley, L. K., & Walter, F. 2001, *Nature* 413: 45–8
- Balbus, S. A. 1995. *Ap. J.* 453:380–3
- Balbus, S. A. 2000. *Ap. J.* 534:420–27
- Balbus, S. A. 2001. *Ap. J.* 562:909–17
- Balbus, S. A. 2002. In *The Physics of Cataclysmic Variables and Related Objects.* eds. B. T. Gänsicke, K. Beuermann, & K. Reinsch. A.S.P., San Francisco. pp. 356–66
- Balbus, S. A., & Hawley, J. F. 1991. *Ap. J.* 376:214–22
- Balbus, S. A., & Hawley, J. F. 1992. *Ap. J.* 392:662–66
- Balbus, S. A., & Hawley, J. F. 1998. *Rev. Mod. Phys.* 70:1–53
- Balbus, S. A., & Hawley, J. F. 2002. *Ap. J.* 573:749–53
- Balbus, S. A., & Terquem, C. 2001. *Ap. J.* 552:235–47
- Balbus, S. A., Hawley, J. F., & Stone J. M. 1996. *Ap. J.* 467:76–86
- Balbus, S. A., & Papaloizou, J. C. B. 1999. *Ap. J.* 521:650–58
- Bayly, B. J., Orszag, S. A., & Herbert, T. 1988. *Ann. Rev. Fluid Mech.* 20:359–91

- Begelman, M. 1978. *MNRAS* 184:53–67
- Binney, J., & Tremaine, S. 1987, *Galactic Dynamics*, Princeton Univ. Press, Princeton
- Blaes, O. M. 1987. *MNRAS* 227:975–92
- Blaes, O. M. 2002. *Physics Fundamentals of Luminous Accretion Disks Around Black Holes*, in “Accretion Disks, Jets, and High Energy Phenomena in Astrophysics”, Proceedings of Session LXXVIII of Les Houches Summer School, Chamonix, France, August 2002, eds. F. Menard, G. Pelletier, G. Henri, V. Beskin, and J. Dalibard EDP Science: Paris and Springer, Berlin, in press (astro-ph/0211368)
- Blaes, O. M., & Balbus, S. A. 1994. *Ap. J.* 421:163–77
- Blaes, O. M., & Scoville, A. 2001. *Ap. J.* 553:987–98
- Blandford, R. D., & Begelman, M. C. 1999. *MNRAS* 303:L1–5
- Brandenburg, A., Nordlund, Å., Stein, R. F., & Torkelsson, U. 1995. *Ap. J.* 446:741–54
- Cabot, W. 1996. *Ap. J.* 465:874–86
- Chandrasekhar, S. 1953. *Proc. Roy. Soc. (London) A* 216:293–309
- Chandrasekhar, S. 1960. *Proc. Nat. Acad. Sci.* 46:253–7
- Chandrasekhar, S. 1961. *Hydrodynamic and Hydromagnetic Instability*, Clarendon Press, Oxford, pp. 402–3
- Coles, D. 1965. *J. Fluid Mech.* 21:385–425
- Corcos, G. M., & Lin, S. J. 1984. *J. Fluid Mech.* 139:67–95
- Crawford, J. A., & Kraft, R. P. 1956. *Ap. J.* 123:44–53
- Fleming, T. P., Stone, J. M., & Hawley, J. F. 2000. *Ap. J.* 530:464–77
- Frank, J., King, A., & Raine, D. 2002. *Accretion Power in Astrophysics*, Cambridge Univ. Press, Cambridge, pp. 104–5
- Fricke, K. 1969. *Astron. Astrophys.* 1:388–98
- Fromang, S., Terquem, C., & Balbus, S. A. 2002 *MNRAS* 329:18–28
- Gammie, C. F. 1996. *Ap. J.* 457:355–62
- Gammie, C. F., & Menou, K. 1998. *Ap. J.* 492:L75–8
- Glassgold, A. E., Feigelson, E. D., & Montmerle, T. 2000. In *Protostars and Planets IV*. eds. V. Mannings, A. P. Boss, & S. S. Russell. Univ. Arizona, Tucson. pp. 429–55
- Goldreich, P., Goodman, J., and Narayan, R. 1986. *MNRAS* 221:339–64
- Goldreich, P., & Tremaine, S. D. 1979. *Ap. J.* 233:857–71
- Goldreich, P., & Tremaine, S. D. 1980. *Ap. J.* 241:425–41
- Goodman, J., & Ji, H. 2002. *J. Fluid Mech.* 462:365–82
- Goodman, J., & Rafikov, R. R. 2001. *Ap. J.* 552:793–802
- Goodman, J., & Xu, G. 1994. *Ap. J.* 432:213–23
- Hartmann, L., Calvet, N., Gullbring, E., & D’Alessio, P. 1998. *Ap. J.* 495:385–400
- Hawley, J. F. 1991. *Ap. J.* 381:496–507
- Hawley, J. F. 2000. *Ap. J.* 528:462–79
- Hawley, J. F. 2001. *Ap. J.* 554:534–47
- Hawley, J. F., & Balbus, S. A. 1992. *Ap. J.* 400:595–609
- Hawley, J. F., & Balbus, S. A. 2002. *Ap. J.* 573:738–48
- Hawley, J. F., Balbus, S. A., & Stone, J. M. 2001. *Ap. J.* 554:L49–52
- Hawley, J. F., Balbus, S. A., & Winters, W. F. 1999. *Ap. J.* 518:394–404
- Hawley, J. F., Gammie, C. F., & Balbus, S. A. 1995. *Ap. J.* 440:742–63
- Hawley, J. F., Gammie, C. F., & Balbus, S. A. 1996. *Ap. J.* 464:690–703

- Hawley, J. F., & Krolik, J. H. 2001. *Ap. J.* 548:348–67
- Hawley, J. F., & Krolik, J. H. 2002. *Ap. J.* 566:164–80
- Hawley, J. F., & Stone, J. M. 1995. *Comp. Phys. Comm.* 89:127–48
- Ichimaru, S. 1977. *Ap. J.* 214:840–55
- Ji, H., Goodman, J., & Kageyama, A. 2001. *MNRAS*, 325, L1–5
- Krolik, J. 1999. *Active Galactic Nuclei*, Princeton University Press, Princeton
- Li, H., Finn, J. M., Lovelace, R. V. E., & Colgate, S. A. 2000. *Ap. J.* 533:1023–34
- Lighthill, J. 1978. *Waves in Fluids*, Cambridge: Cambridge Univ. Press
- Lin, D. N. C., & Papaloizou, J. C. B. 1979. *MNRAS* 188:191–201
- Longaretti, P.-Y. 2002. *Ap. J.* 576:587–98
- Lovelace, R. V. E., Li, H., Colgate, S. A., & Nelson, A. F. 1999. *Ap. J.* 513:805–10
- Lynden-Bell, D. 1969. *Nature* 223:690–94
- Lynden-Bell, D., & Kalnajs, A. J. 1972. *MNRAS* 157:1–30
- Lynden-Bell, D., & Pringle, J. E. 1974. *MNRAS* 168:603–37
- Machida, M., Hayashi, M. R., & Matsumoto, R. 2000. *Ap. J.* 532:L67–70
- Matsumoto, R., & Tajima, T. 1995. *Ap. J.* 445:767–79
- Menou, K., & Quataert, E. 2001. *Ap. J.* 552:204–8
- Miller, K. A., & Stone, J. M. 2000. *Ap. J.* 534:398–419
- Moffatt, K. 1978, *Magnetic Field Generation in Electrically Conducting Fluids*. Cambridge University Press, Cambridge
- Narayan, R. 2002. In *Lighthouses of the Universe: The Most Luminous Celestial Objects and Their Use for Cosmology, Proceedings of the MPA/ESO*, eds. M. Gilfanov, R. Sunyaev, E. Churazov, pp. 405–29. Berlin: Springer-Verlag
- Narayan, R., Igumenshev, I. V., & Abramowicz, M. A. 2000, *ApJ*, 539, 798
- Narayan, R., Mahadevan, R., & Quataert, E. 1998. In *Theory of Black Hole Accretion Disks*, eds. M. A. Abramowicz, G. Bjornsson, and J. E. Pringle, Cambridge University Press, Cambridge. pp. 148–73
- Narayan, R., Quataert, E., Igumenshev, I. V., & Abramowicz, M. A. 2002. *Ap. J.* 577:295–301
- Narayan, R., & Yi, I. 1994. *Ap. J.* 428:L13–16
- Narayan, R., & Yi, I. 1995. *Ap. J.* 452:710–35
- Nelson, R. P., & Papaloizou, J. C. B. 2002, astro-ph/0211495
- Newcomb, W. A. 1962. *Nuc. Fusion: 1962 Suppl., Part 2*. pp. 451–63
- Noguchi, K., Pariev, V. I., Colgate, S. A., Beckely, H. F., & Nordhaus, J. 2002. *Ap. J.* 575:151–62
- Ogilvie, G. I., & Lubow, S. H. 1999. *Ap. J.* 515:767–75
- Ogilvie, G. I., & Proctor, M.R. E. 2003. *J. Fluid Mech.* 476:389–409
- Orszag, S. A., & Patera, A. T. 1980. *Phys. Rev. Lett.* 45:989–93
- Orszag, S. A., & Patera, A. T. 1981. In *Transition and Turbulence*, ed. R. E. Meyer, pp. 127–46. New York: Academic
- Paczynski, B., & Wiita, P. J. 1980. *Astron. Astrophys.* 88:23–31
- Papaloizou, J. C. B., & Pringle, J. E. 1984. *MNRAS* 208:721–50
- Papaloizou, J. C. B., & Pringle, J. E. 1985. *MNRAS* 213:799–820
- Papaloizou, J. C. B., & Terquem, C. 1995. *MNRAS* 274:987–1001
- Pierrehumbert, R. T., & Widnall, S. E. 1982. *J. Fluid Mech.* 114:59–82
- Pringle, J. E., & Rees, M. J. 1972, *AA*, 21, 1
- Richard, D., & Zahn J.-P. 1999. *Astron. Astrophys.* 347:734–38
- Rüdiger, G., & Shalybkov, D. 2002, *Phy. Rev. E* 66:016307-(1–8)
- Sano, T., & Stone, J. M. 2002. *Ap. J.* 570:314–28
- Shakura, N. I., & Sunyaev, R. A. 1973. *Astron. Astrophys.* 24:337–55

- Shu, F. H. 1992. *The Physics of Astrophysics. Gas Dynamics*. University Science, Sausalito
- Steinacker, A., & Henning, T. 2001. *Ap. J.* 554:514–27
- Steinacker, A., & Papaloizou, J. C. B. 2002. *Ap. J.* 571:413–28
- Stone, J. M., & Balbus, S. A. 1996. *Ap. J.* 464:364–72
- Stone, J. M., Hawley, J. F., Gammie, C. F., & Balbus, S. A. 1996. *Ap. J.* 463:656–73
- Stone, J. M., & Pringle, J. E. 2001. *MNRAS* 322:461–72
- Tassoul, J. L. 1978. *Theory of Rotating Stars*, Princeton Univ. Press, Princeton
- Terquem, C., & Papaloizou, J. C.B. 1996. *MNRAS* 279:767–84
- Triton, D. J. 1988. *Physical Fluid Dynamics*, Clarendon Press, Oxford
- Turner, N. J., Stone, J. M., & Sano, T. 2002. *Ap. J.* 566:148–63
- Uchida, Y., & Shibata, K. 1985. *PASJ* 35:515–35
- Umebayashi, T., & Nakano, T. 1988. *Prog. Theo. Phys. Suppl.* 96:151–60
- Varnière, P., & Tagger, M. 2002. *Astron. Astrophys.* 394:329–38
- Velikhov, E. P. 1959. *J. Expl. Theoret. Phys. (U.S.S.R.)* 36:1398–1404
- Vishniac, E. T., & Diamond, P. 1989. *Ap. J.* 347:435–47
- Ward, W. R. 1986. *Icarus* 67:164–80
- Ward, W. R. 1997. *Icarus* 126:261–81
- Wardle, M. 1999. *MNRAS* 307:849–56
- Wardle, M., & Königl, A. 1993. *Ap. J.* 410:218–38
- Zahn, J.-P., Toomre, J., Spiegel, E. A. 1974. *J. Fluid Mech.* 64:319–45

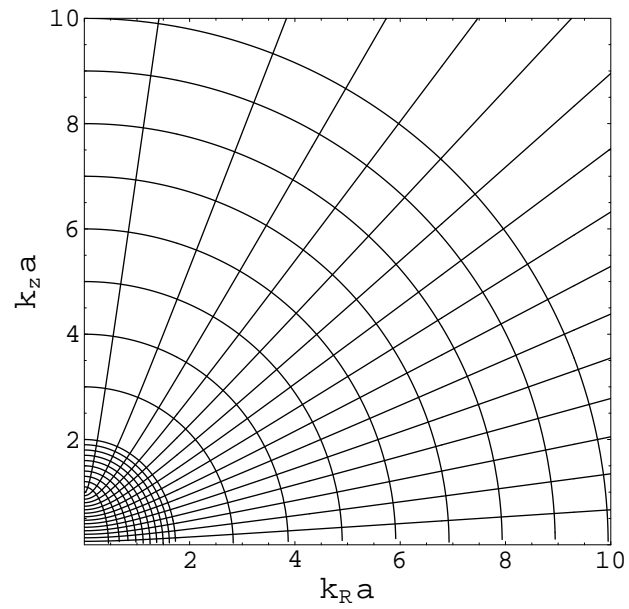


Figure 1: Contours of constant $\bar{\omega}$ for the dispersion relation (30) of a Keplerian disk. These form a set of conformal ellipses (density waves) and hyperbolae (inertial waves). The value of $\bar{\omega}$ along a curve is read off at the point of intersection with the $k_R = 0$ axis; the numerical scale is in units of $\Omega = 1$. Density wave ellipses are separated by one unit for $\bar{\omega} > 2$ and 0.1 units for $1.1 < \bar{\omega} < 2$. Inertial wave hyperbolae are separated by .066 units.

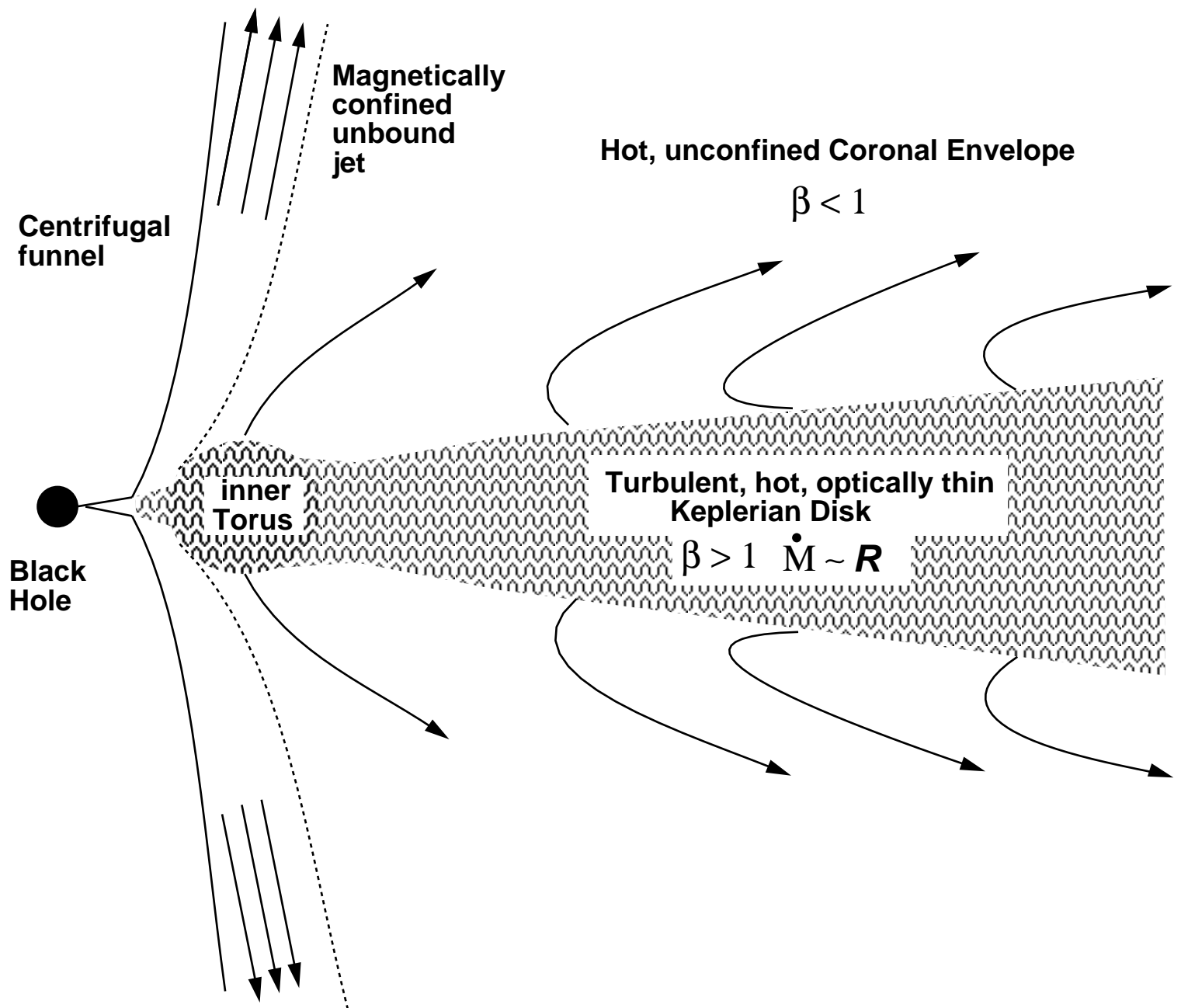


Figure 2: A schematic diagram of a nonradiative accretion flow, highlighting its principal features. A turbulent, nearly Keplerian gas-dominated hot disk is surrounded by an active, diffuse, magnetic-dominated coronal envelope. Near the marginally stable orbit, the flow thickens into a small inner torus. A centrifugally-evacuated funnel lies along the axis, surrounded by a jet confined by magnetic pressure in the corona. From Hawley & Balbus (2002).